

THE 160 SQUARE DEGREE *ROSAT* SURVEY: THE REVISED CATALOG OF 201 CLUSTERS WITH SPECTROSCOPIC REDSHIFTS¹

C.R. MULLIS^{2,3}, B.R. MCNAMARA^{4,5}, H. QUINTANA⁶, A. VIKHLININ⁵, J.P. HENRY³, I.M. GIOIA^{7,3},
A. HORNSTRUP⁸, W. FORMAN⁵, AND C. JONES⁵
Accepted for publication in ApJ

ABSTRACT

We present the revised catalog of galaxy clusters detected as extended X-ray sources in the 160 Square Degree *ROSAT* Survey, including spectroscopic redshifts and X-ray luminosities for 200 of the 201 members. The median redshift is $z_{\text{median}} = 0.25$ and the median X-ray luminosity is $L_{X,\text{median}} = 4.2 \times 10^{43} \text{ h}_{50}^{-2} \text{ erg s}^{-1}$ (0.5–2.0 keV). This is the largest high-redshift sample of X-ray selected clusters published to date. There are 73 objects at $z > 0.3$ and 22 objects at $z > 0.5$ drawn from a statistically complete flux-limited survey with a median object flux of $1.4 \times 10^{-13} \text{ erg cm}^{-2} \text{ s}^{-1}$. We describe the optical follow-up of these clusters with an emphasis on our spectroscopy which has yielded 155 cluster redshifts, 110 of which are presented here for the first time. These measurements combined with 45 from the literature and other sources provide near-complete spectroscopic coverage for our survey. We discuss the final optical identifications for the extended X-ray sources in the survey region and compare our results to similar X-ray cluster searches.

Subject headings: catalogs — galaxies: clusters: general — surveys — X-rays: galaxies

1. INTRODUCTION

According to the theory of hierarchical structure formation, clusters of galaxies are amongst the largest and most recent systems to form in the matrix of cosmic construction (e.g., Peebles 1993; Peacock 1999). Measurements based on dynamical, gravitational lensing, and X-ray data independently confirm the extreme magnitude of cluster masses (10^{14} – $10^{15} M_{\odot}$); thus situating them as the largest virialized masses in the Universe (e.g., Smail et al. 1997; Wu et al. 1998; Allen et al. 2001; Clowe & Schneider 2002). Observed phenomena including cluster-cluster mergers, shock fronts, infalling sub-clusters, and non-spherical morphologies attest to the on-going assembly of clusters. (e.g., Gioia et al. 1999; Vikhlinin, Markevitch, & Murray 2001; Czoske et al. 2002; Markevitch et al. 2002; Rose et al. 2002).

As galaxy clusters form in the deepest gravitational potentials, presumably at the intersections of filaments in the “cosmic web” of large-scale structure, they are excellent tracers of the matter distribution in the Universe (e.g., Bond, Kofman, & Pogosyan 1996; Jenkins et al. 1998; Mullis et al. 2001; Borgani & Guzzo 2001). Moreover, clusters are important tools for constraining cosmological parameters. For example, determinations of the mass, X-ray luminosity, and X-ray temperature functions can be used to measure the matter density parameter (Ω_M) and the amplitude (σ_8) of density fluctuations (e.g., Henry 2000; Borgani et al. 2001; Vikhlinin et al. 2003). Observations of the Sunyaev-Zeldovich (SZ) effect combined with

X-ray imaging of clusters can be used to assess the Hubble parameter (H_0) via a technique notably independent of the distance ladder (e.g., Sunyaev & Zeldovich 1972; Silk & White 1978; Carlstrom, Holder, & Reese 2002;). By no means is this overview of systemic cluster applications complete; see the reviews, and references therein, of Sarazin (1988) for a historical perspective on cluster X-ray emission, Mulchaey (2000) for the X-ray properties of galaxy groups, and Rosati, Borgani, & Norman (2002) for the current understanding of evolutionary trends in X-ray clusters of galaxies.

The significance of galaxy clusters and the strong interest to discover and investigate these remarkable structures are demonstrated by the sheer number of surveys undertaken in recent years. In the high-energy domain alone, there are at least sixteen independent X-ray-selected cluster surveys spanning the *Einstein* and *ROSAT* eras (see Table 1). X-ray selection is currently the optimal procedure for building cluster samples with minimum bias and maximum statistical completeness. Techniques currently under development that may offer a competitive alternative include gravitational lensing and SZ surveys. Rosati et al. (2002) provide a detailed discussion of X-ray survey strategies, and Postman (2002) offers a comprehensive comparison of the X-ray, optical/NIR, and SZ approaches.

We briefly review the basic properties of cluster X-ray emission. On megaparsec scales dark matter halos collapse pulling in gas and galaxies. This gas comprises $\sim 85\%$ of the luminous cluster mass, and is heated to several 10^7 K

¹ Based on observations obtained at the W.M. Keck Observatory, jointly operated by the California Institute of Technology, the University of California and the National Aeronautics and Space Administration, at the University of Hawai'i 2.2 m telescope, and at the European Southern Observatory 3.6 m on La Silla (ESO Programs 60.A-0694, 62.O-0586, 64.O-0455).

² European Southern Observatory, Headquarters, Karl-Schwarzschild-Strasse 2, Garching bei München D-85748, Germany, cmullis@eso.org

³ Institute for Astronomy, University of Hawai'i, 2680 Woodlawn Drive, Honolulu, HI 96822, USA

⁴ Department of Physics and Astronomy, Ohio University, Athens, OH 45701, USA

⁵ Harvard-Smithsonian Center for Astrophysics, 60 Garden Street, Cambridge, MA 02138, USA

⁶ Departamento de Astronomia y Astrofísica, Pontificia Universidad Católica de Chile, Casilla 104, Santiago, 22, Chile

⁷ Istituto di Radioastronomia del CNR, via Gobetti 101, Bologna, I-40129, Italy

⁸ Danish Space Research Institute, Juliane Maries Vej 30, Copenhagen 0, DK-2100, Denmark

through adiabatic compression and shock heating during cluster formation. At these extreme temperatures the gas is highly ionized, optically thin ($n \sim 10^{-3} \text{ cm}^{-3}$), and primarily radiates via thermal bremsstrahlung with minor contributions from thermal line transitions (e.g., 6.7 keV Fe $K\alpha$).

The X-ray advantages of cluster selection are impressive. Clusters are very luminous (10^{43} – $10^{45} \text{ erg s}^{-1}$) and spatially *extended* X-ray sources, which are efficiently detectable to high redshifts (e.g., RX J0848.9+4452 at $z = 1.26$, Rosati et al. 1999; Stanford et al. 2001). Since the X-ray emission is proportional to the gas density squared, clusters have relatively peaked surface-brightness profiles. This characteristic coupled with the low X-ray background nearly eliminates projection effects and underpins the high statistical quality of X-ray samples. The cosmological utility is further enhanced by the strong correlation of X-ray luminosity with cluster mass, and the fact that X-ray surveys feature well-defined selection functions. The latter is critical for reliably transforming source counts to volume-normalized diagnostics.

In this paper we present the spectroscopic redshift catalog for the 160 Square Degree *ROSAT* Cluster Survey (hereafter 160SD). The 201 galaxy clusters of the 160SD survey represent the largest, high-redshift X-ray selected sample published to date. First described by Vikhlinin et al. (1998a, hereafter V98), the 160SD clusters have been used to study the evolution of cluster X-ray luminosities and radii (Vikhlinin et al. 1998b), to present evidence for a new class of X-ray overluminous elliptical galaxies or “fossil groups” (Vikhlinin et al. 1999), to analyze the correlation of optical cluster richness with redshift and X-ray luminosity (McNamara et al. 2001), and to discover gravitational lenses (Muñoz et al. 2001; Hornstrup et al. 2003). *Chandra* observations of high-redshift 160SD clusters have been used to make an accurate determination of the evolution of the scaling relations between X-ray luminosity, temperature, and gas mass (Vikhlinin et al. 2002), and to derive cosmological constraints from the evolution of the cluster baryon mass function (Vikhlinin et al. 2003). The most recent results are reported by Mullis et al. (2003) who find significant evolution in the number density of clusters as a function of redshift based on number counts and changes in the X-ray luminosity functions.

In §2 we review the design of the 160SD survey and describe the optical follow-up observations with an emphasis on the new spectroscopy. In §3 we present the revised cluster catalog which features essentially complete spectroscopic redshifts. We describe the general properties of our cluster sample and compare them to the results of other X-ray surveys in §4. We close with a brief summary in §5. Throughout this analysis we assume an Einstein-de Sitter cosmological model with $H_0 = 50 \text{ h}_{50} \text{ km s}^{-1} \text{ Mpc}^{-1}$ and $\Omega_M = 1$ ($\Omega_\Lambda = 0$), and quote X-ray fluxes and luminosities in the 0.5–2.0 keV energy band.

2. THE 160 SQUARE DEGREE ROSAT SURVEY

The study of high-redshift galaxy clusters was revolutionized by the *ROSAT* X-ray satellite (Trümper 1993) which was used to perform the first all-sky survey with an imaging X-ray telescope and to carry out a program of deep pointed observations for nearly a decade (1990–

1999). These data, the *ROSAT* All-Sky Survey (RASS, Voges 1992) and the archive of pointed observations, are the basis of many X-ray selected surveys which have identified more than 1000 clusters; survey acronyms and principal references are given in Table 1. See Rosati et al. (2002) for an extensive review of the subject.

Applying different combinations of solid angle and X-ray flux sensitivity, the *ROSAT* cluster surveys provide good coverage of the X-ray luminosity-redshift parameter space. For example, BCS, CIZA, NORAS, and REFLEX adopted the wide ($\sim 10^4 \text{ deg}^2$) and shallow ($f_X \gtrsim 3 \times 10^{-12} \text{ erg cm}^{-2} \text{ s}^{-1}$) strategy using the RASS data to locate relatively nearby clusters ($z \lesssim 0.3$). Conversely surveys such as BMW-HRI, RDCS, SSHARC, and WARPS executed deep searches ($f_X \gtrsim 2\text{--}6 \times 10^{-14} \text{ erg cm}^{-2} \text{ s}^{-1}$) with more modest solid angles ($\sim 20\text{--}200 \text{ deg}^2$) to identify higher redshift clusters. Our 160SD survey falls into the latter category. In the following section we review the design of the program and elaborate on the optical follow-up observations. See V98 for a complete description of the 160SD survey methodology.

2.1. X-ray Selection of Cluster Candidates

Clusters of galaxies are rare occurrences in the X-ray sky. Surveys such as the EMSS and NEP which have rigorously identified *all* X-ray sources within their survey regions find only $\sim 12\text{--}15\%$ of the X-ray emitters at high Galactic latitudes are clusters (Stocke et al. 1991; Henry et al. 2001; Mullis 2001; Gioia et al. 2003). However, except for nearby, isolated elliptical galaxies, clusters are essentially the only extended X-ray sources away from the Galactic Plane. Thus with X-ray imaging data of sufficient spatial resolution and signal-to-noise, X-ray extent is an excellent means to efficiently identify galaxy clusters.

The 160SD clusters were selected based on the serendipitous detection of extended X-ray emission in 647 archival *ROSAT* PSPC observations. The search included all fields with Galactic latitude $|b| > 30^\circ$ and hydrogen column densities $n_H < 6 \times 10^{20} \text{ cm}^{-2}$ but excluded 10° radius regions around the SMC and LMC. PSPC observations targeting known clusters of galaxies, nearby galaxies, star clusters, and supernova remnants were not analyzed. A total of 160 deg^2 were surveyed at high fluxes. At lower fluxes, the sky coverage smoothly decreases due to the survey selection function (see Table 5 in V98). The area drops to 80 deg^2 at the median survey flux ($1.2 \times 10^{-13} \text{ erg cm}^{-2} \text{ s}^{-1}$) and to 5 deg^2 at $3.7 \times 10^{-14} \text{ erg cm}^{-2} \text{ s}^{-1}$ (which is the effective lower flux limit of the survey).

Operating on hard-band images (0.6–2.0 keV), a wavelet decomposition algorithm was used to detect X-ray sources between $2.5'$ and $17.5'$ from the PSPC field center. The inner radius allows for the avoidance of the original target of the pointing and the outer radius is set by the window support structure of *ROSAT* PSPC. X-ray sources significantly broader than the point-spread function (PSF), as determined through a maximum-likelihood determination, qualified for the initial list of candidate galaxy clusters.

The PSF of the *ROSAT* PSPC has a FWHM of about $25''$ on-axis which grows to about $45''$ at $17.5'$ off axis. The radial surface-brightness profile of cluster X-ray emission is characterized by a β -model, $I(r, r_c) = I_0(1 + r^2/r_c^2)^{-3\beta+0.5}$ (Cavaliere & Fusco-

Femiano 1976). A cluster with the canonical properties (core radius $r_c=250 h_{50}^{-1}$ kpc and slope $\beta = 2/3$) at $z = 1$ corresponds to an angular radius of $\sim 30''$ or a FWHM of $\sim 60''$ and thus is easily resolved in our survey. For a more stringent scenario consider $r_c=100 h_{50}^{-1}$ kpc which is at the very low end of the observed distribution of core radii (e.g., Jones & Forman 1999). At $z = 1$ the intrinsic radius is $\sim 12''$. Nonetheless the convolution of the intrinsic profile and the PSF results in a significantly extended source even for this compact cluster at high redshift. The decreased detection probability for such a small cluster at larger off-axis angles is incorporated into the 160SD selection function.

It is important to recognize that though X-ray extent is the primary selection criterion for our survey, comparisons with other surveys (e.g., WARPS, Perlman et al. 2002) demonstrate that no clusters were missed as unresolved sources. Hence the results of the 160SD survey are in effect a statistically complete, X-ray flux-limited cluster sample.

2.2. Initial Optical Follow-up Observations

Following the X-ray selection of 223 candidate clusters, optical observations are required to verify the presence of a galaxy cluster and to estimate the distance to each system. V98 described the initial phase of these follow-up observations. A search of the NASA/IPAC Extragalactic Database (NED⁹) revealed 37 previously known clusters, 31 of which had measured redshifts in the literature. For the remaining 186 candidates, photometric CCD imaging in the *R*-band was obtained using the Fred Lawrence Whipple Observatory (FLWO) 1.2m, European Southern Observatory (ESO) / Danish 1.54m, and Las Campanas 1m telescopes. These were supplemented in the case of seven bright clusters using the DSS-II plates which can be used to identify clusters to $z \lesssim 0.45$. The CCD imaging was sufficiently deep to reveal clusters to $z = 0.7 - 0.9$. Figure 1 illustrates the relative ease of establishing the presence of distant clusters even with short exposures through a modest telescope. An overdensity of galaxies visible in this 5 minute *R*-band image from the FLWO 1.2m is perfectly aligned with the X-ray emission from an 80 ks *Chandra* observation. Our subsequent Keck-II longslit spectra (Figure 2) taken along the major axis of the X-rays and galaxy distribution confirm the presence of a cluster at $z = 0.700$. If a concentration of galaxies is not present in the CCD imaging it was classified as a false detection though it could presumably be a very distant cluster (e.g., RX J0848.9+4452 which is 160SD cluster #61 at $z = 1.26$).

In total 203 clusters were confirmed by V98 (see Table 2). Of the remaining 20 sources, 19 are probable false detections resulting from the blends of unresolved X-ray point sources. It was not possible to confirm RX J1415.6+1906 (#157) because it is obscured by the glare of Arcturus. The exceptional quality of the 160SD X-ray selection is reinforced by this high success rate (91%).

The second phase of the optical follow-up concerns spectroscopic measurements principally used to measure distances to the clusters. Of course the determination of concordant redshifts from amongst the likely

cluster members further justifies the cluster classification, but this is somewhat ancillary given the presence of extended X-ray emission spatially coincident with a galaxy density enhancement. As previously noted, spectroscopic redshifts for 31 of the clusters were available from the literature. V98 obtained spectroscopic redshifts for 45 additional clusters using the Multiple Mirror Telescope 6×1.8m, ESO 3.6m, and ESO/Danish 1.54m telescopes, and presented photometric redshifts for 124 of the remaining 127 clusters based on the magnitude of the brightest cluster galaxy (BCG). Reliable photometric estimates were not possible for three candidates RX J0910.6+4248 (#69), RX J1237.4+11141 (#122), and RX J1438.9+6423 (#164) because the selection of the BCG in each case was unclear due to the large angular extent of the candidate. Note the object identification numbers in parentheses are the same as the ones used in V98. The distance estimates of V98 are summarized in the second column of Table 3.

The membership of the 160SD cluster sample has proven to be remarkably stable since first presented by V98. Based on the results of extensive spectroscopic follow-up (described in §2.3), the revised sample consists of 201 confirmed clusters, 21 false detections, and one source obscured by Arcturus (see Table 2). These classifications have changed very little; one probable false detection has been identified as a cluster and three cluster candidates have been reclassified as probable falses. RX J0848.9+4452 (#61) was originally classified as a probable false detection because no galaxy overdensity was visible in our optical image of this field. However, it was forewarned that such an object could be a very distant ($z \gtrsim 0.9$) cluster. In fact Rosati et al. (1999) have proven that this X-ray source is a cluster at $z = 1.26$ making it the most distant system found in any of the X-ray surveys thus far. RX J0857.7+2747 (#65), RX J1429.6+4234 (#163), and RX J2004.8-5603 (#197) were initially cluster candidates but we now interpret them to be likely false detections because our spectroscopic survey of these fields failed to find any coherent structure in redshift space.

2.3. New Spectroscopic Redshifts

Since the initial follow-up observations we have gone on to measure spectroscopic redshifts for 110 additional clusters from our 160SD survey using the Keck-II 10m and the University of Hawai'i (UH) 2.2m telescopes at the Mauna Kea Observatories, and the ESO 3.6m telescope at La Silla Observatory. Combining these new redshifts with 76 measurements reported by V98 and 14 redshifts from the literature and private communications results in essentially complete (200 of 201 clusters) spectroscopic coverage for our entire sample. Refer to Table 3 for a summary of the redshift determinations. The new cluster catalog will be presented in §3. Here we give a technical description of the new observations.

We chose the targets for the low-dispersion spectroscopic observations using our previously described CCD images. This was usually a straightforward task since in most cases unambiguous cluster members were spatially coincident with the extended X-ray emission. Longslit spectra were obtained with the Keck-II 10m and the UH 2.2m resulting

⁹ <http://nedwww.ipac.caltech.edu/>

in usually 2–3 concordant galaxy redshifts per cluster, and always including the BCG. Longslit and multi-object spectra were taken with the ESO 3.6m, the latter producing 10–15 galaxy redshifts per cluster.

We measured redshifts for the most distant clusters ($z \gtrsim 0.5$) using the Keck-II 10m telescope with the Low Resolution Imaging Spectrometer (LRIS, Oke et al. 1995) during four nights of observations (1999 July 07–08 and 2000 January 26–27). Examples are shown in Figures 2 and 4. The 300 lines mm^{-1} grating (5000Å blaze) combined with the GG495 long-pass order-blocking filter yielded an effective wavelength coverage of approximately 5000Å–9000Å and a dispersion of 2.45Å pixel^{-1} . With the Tektronix 2048×2048 CCD detector the spatial scale is $0.215'' \text{ pixel}^{-1}$. We used a slit of $1.5''$ in width, which gives a reduced spectral resolution of $\sim 16\text{Å FWHM}$ ($R \sim 440$). Exposure times were typically 1200s–2400s and the seeing was $0.7''$ – $1.1''$.

Moderately distant clusters were observed using the UH 2.2m with the Wide Field Grism Spectrograph (WFGS) during ten nights of spectroscopy (1998 May – 2000 February). The instrument setup consisted of the Tektronix 2048×2048 CCD at the f/10 focus with the 420 lines mm^{-1} red grism and a $1.8''$ slit, providing a wavelength coverage of approximately 3800Å–9000Å. The spectral dispersion is 3.6Å pixel^{-1} , the spectral resolution is $\sim 19\text{Å FWHM}$ ($R \sim 340$), and the spatial scale is $0.35'' \text{ pixel}^{-1}$. The typical seeing was $0.8''$ – $1.5''$ and integration times ranged between 600s and 3600s.

We observed the southern clusters not visible from Mauna Kea using the ESO 3.6m with the ESO Faint Object Spectrograph and Camera (EFOSC2), in both the longslit and the multi-object spectroscopy modes. Data were taken over 6 nights (1998 March 28, 1999 February 15–16, and 1999 November 06–08) during which time the seeing varied over the range $0.6''$ – $1.8''$. The 300 lines mm^{-1} grating (#6, 5000Å blaze) with a $1.5''$ slit provides a wavelength coverage of about 3900Å–8000Å with a spectral resolution of $\sim 20\text{Å}$ ($R \sim 300$). The spectral dispersion is 4Å pixel^{-1} and the spatial scale is $0.31'' \text{ pixel}^{-1}$ using the Loral 2048×2048 CCD binned 2×2 at readout. Exposure times were usually between 900s and 1800s.

In total we observed over 400 individual galaxies to derive the 110 new cluster redshifts reported in this paper. The only cluster for which we lack a redshift is RX J1237.4+1141 (#122). The unusually large extent of this source would require an extensive redshift survey to yield a reliable distance measurement. We analyzed our data following standard procedures using IRAF¹⁰ reduction packages and IDL¹¹ routines. Two-dimensional spectra were de-biased and flat-fielded. One-dimensional spectra, with the sky background subtracted, were extracted and wavelength calibrated. Finally the instrumental response was removed using observations of the spectrophotometric standard stars of Oke & Gunn (1983) and Massey et al. (1988). Redshifts were measured based on the offsets of absorption features commonly observed in early-type galaxies including the Ca II H and K doublet (3933.68Å,

3968.49Å), the 4000Å break, the CH G band ($\sim 4300\text{Å}$), Mg Ib ($\sim 5175\text{Å}$), and Na Id (5889.97Å).

Brief descriptions of a few individual clusters demonstrate the reliability of our X-ray source characterization and the rigor of our optical follow-up program. Though relatively simple X-ray/optical configurations such as that shown in Figure 1 are the most commonly observed, there are more challenging scenarios. Take for instance the 160SD source RX J0921.2+4528 (#70). We were surprised when our spectrum of the apparent BCG revealed a broad-line QSO at $z = 1.66$. Since active galactic nuclei (AGN) are usually X-ray luminous we could have stopped here and classified RX J0921.2+4528 as an AGN. However our analysis of the X-ray data shows this source is significantly (6σ) broader than the ROSAT PSPC PSF thus motivating us to pursue this further. With subsequent spectroscopy we found five concordant redshifts at $z = 0.315$ confirming the cluster identification. More interestingly, a second QSO at $z = 1.66$ was found separated $6.93''$ from the first. Muñoz et al. (2001) further describe this wide-separation gravitational lens candidate. Our Monte-Carlo simulations show that a 90% upper limit on the flux of a point source at the QSO position is about 35% of the total cluster flux.

Another complex source to disentangle is RX J1524.6+0957 (#170). With a cursory inspection of the *I*-band image shown in Figure 3 one might conclude the obvious low-redshift group is the optical counterpart of the X-ray source. This interpretation was reported by the BSHARC survey who quoted a redshift of $z = 0.078$ (Romer et al. 2000). However, closer scrutiny of the fainter objects suggests a concentration of galaxies at the X-ray position. Our Keck-II spectroscopy for these faint galaxies establishes a distant cluster at $z = 0.516$ (Figure 4). Were the nearby group the principal source of the X-rays, it would have to be exceedingly compact. The measured core radius of $26''$ corresponds to $52 h_{50}^{-1} \text{ kpc}$ at $z = 0.078$ or $190 h_{50}^{-1} \text{ kpc}$ at $z = 0.516$. The former is unrealistic whereas the latter is quite typical. Finally, we measure an $\sim 5 \text{ keV}$ temperature for the intracluster medium, via a spectral fit to the *Chandra* data, which strongly rejects the group-dominant scenario. Thus we conclude the primary identification for RX J1524.6+0957 is a distant cluster at $z = 0.516$.

We close this section with an assessment of the photometric redshift estimates of V98 versus the spectroscopic measurements reported here. Looking at the relevant data plotted in Figure 5 we see that in general the photometric redshifts were quite reliable. In retrospect the 90% confidence interval of $\Delta z = \begin{smallmatrix} +0.04 \\ -0.07 \end{smallmatrix}$ for the 117 CCD-based estimates was somewhat underestimated by V98, since only 70% of the spectroscopic redshifts actually fall within this error range. Ignoring the six principal outliers labeled in Figure 5, the true 90% confidence interval is about $\Delta z = \pm 0.1$.

3. REVISED CLUSTER CATALOG WITH SPECTROSCOPIC REDSHIFTS AND X-RAY LUMINOSITIES

We present the revised cluster catalog for the 160SD survey in Table 4. The most significant feature is the nearly

¹⁰ IRAF is distributed by the National Optical Astronomy Observatories, which are operated by the Association of Universities for Research in Astronomy, Inc., under cooperative agreement with the National Science Foundation. <http://iraf.noao.edu>

¹¹ <http://www.rsinc.com>, <http://idlastro.gsfc.nasa.gov/homepage.html>

complete spectroscopic coverage. We report spectroscopic redshifts for 200 of the 201 (99.5%) clusters in our sample. With knowledge of the cluster distances we can compute accurate X-ray luminosities. Hence the fundamental parameters are now available to pursue detailed investigations with this statistically complete, X-ray flux-limited sample.

In Table 4 we provide detailed information for each of the 201 clusters discovered in the 160SD survey. For completeness we also list the 22 other objects meeting our original selection criteria of significant X-ray extent. Twenty-one of these, flagged with “F” in columns (10), (11), and (13), are likely false detections due to blends of unresolved X-ray point sources. The other source is only 4.4′ away from the zero magnitude star Arcturus and hence nearly impossible to confirm as a cluster.

The object name and object number are given in columns (1) and (2). Note the latter is the same identification used by V98. The right ascension and declination (J2000) for the centroid of the X-ray emission are listed in columns (3) and (4). Column (5) gives the positional uncertainty in terms of the radius for the 90% confidence X-ray position error circle. Columns (6) and (7) give the angular core radius and its uncertainty based on a β -model fit with $\beta = 2/3$. The total, unabsorbed X-ray flux in the 0.5–2.0 keV energy band in the observer’s restframe and its uncertainty are listed in columns (8) and (9).

Cluster X-ray luminosity in the 0.5–2.0 keV energy band is reported in column (10). Luminosity in the object’s rest frame is defined by

$$L_X = 4\pi d_L^2 f_X k_{0.5-2.0} \quad (1)$$

where f_X is the total X-ray flux, d_L is the luminosity distance (e.g., Weinberg 1972), and $k_{0.5-2.0}$ is the K -correction in the 0.5–2.0 keV band. The latter transforms the *ROSAT* rest-frame luminosity into the object’s rest-frame luminosity. The K -correction here is given by

$$k_{0.5-2.0} = \frac{\int_{0.5}^{2.0} f_E dE}{\int_{0.5(1+z)}^{2.0(1+z)} f_E dE} \quad (2)$$

where f_E is the differential flux (flux per unit energy) as a function of energy and the integration limits are energy band edges in keV. The K -corrections for clusters, shown in Figure 6, were computed assuming a Raymond-Smith plasma spectrum (Raymond & Smith 1977) with a metallicity of 0.3 solar and a gas temperature for the intracluster medium (ICM) consistent with the L_X - kT relation of White, Jones, & Forman (1997),

$$kT = 2.76 \text{ keV } L_{X,\text{bol},44}^{0.33}, \quad (3)$$

where $L_{X,\text{bol},44}$ is the bolometric X-ray luminosity in units of $10^{44} \text{ erg s}^{-1}$ with $H_0 = 50 \text{ h}_{50} \text{ km s}^{-1} \text{ Mpc}^{-1}$

Heliocentric spectroscopic redshifts which entirely supersede the photometric estimates of V98 are given in column (11). We measured redshifts for 155 clusters while 45 come from the literature and private communications as referenced in column (12). In a few cases the precision of literature-based redshifts reported by V98 have been updated to reflect more robust measurements that are now available.

The final column (13) lists notes on individual clusters. In particular we indicate where our 160SD clusters are also

members of other X-ray selected samples. Coincidences were found with the BCS+eBCS (Ebeling et al. 1998, 2000), BMW-HRI (L. Guzzo, priv. comm.), BSHARC (Romer et al. 2000), EMSS (Gioia & Luppino 1994), NORAS (Böhringer et al. 2000), RBS (Schwope et al. 2000), RDCS (P. Rosati, priv. comm.), REFLEX-I/II (H. Böhringer, priv. comm.), RIXOS (Mason et al. 2000), SSHARC (Burke et al. 2003), and WARPS-I/II (Perlman et al. 2002; L. Jones, priv. comm.). No matches were found in the MACS (H. Ebeling, priv. comm.), the NEP (Mullis 2001; Gioia et al. 2003), RASS1BS (De Grandi et al. 1999) or the SGP (Cruddace et al. 2002, 2003) samples.

We also mark in column (13) the four X-ray overluminous elliptical galaxies (OLEGs) described by Vikhlinin et al. (1999) which are potential “fossil groups” similar to those reported by others (e.g., Jones, Ponman, & Forbes 2000, Romer et al. 2000, Mullis 2001). Finally, we note nine instances where the cluster redshift is within $\Delta z = 0.015$ of the original target of the *ROSAT* PSPC pointed observations (flagged with “ z_{PSPC} ”).

4. DISCUSSION

We describe here the general properties of our cluster sample and compare them to the results of other X-ray surveys. In Figure 7 we plot the luminosity-redshift distribution for 160SD clusters. The median redshift is $z_{\text{median}} = 0.25$ and the median X-ray luminosity is $L_{X,\text{median}} = 4.2 \times 10^{43} \text{ h}_{50}^{-2} \text{ erg s}^{-1}$. Note that the 160SD sample is the largest high-redshift sample of X-ray-selected clusters published to date. For example there are 73 clusters at $z > 0.3$ and 22 clusters at $z > 0.5$.

As remarked by Vikhlinin et al. (2003) the *ROSAT* fluxes (and by inference luminosities) used in our survey construction show very good agreement with those measured in deep *Chandra* observations. For the six 160SD clusters observed by both X-ray telescopes (as of early 2003), the fluxes differ by $\leq 13\%$, with no systematic offset, and always within the statistical uncertainties. Comparisons of fluxes independently measured from *ROSAT* observations demonstrate consistent results. For example, using appropriate core radii and redshifts, Romer et al. (2000) report no systematic offsets between their measurements and ours for 11 clusters which are common to the BSHARC and 160SD surveys. Examining 16 clusters detected in the 20 *ROSAT* fields surveyed by both WARPS-I and 160SD, Perlman et al. (2002) find a mean flux ratio of $f_{160\text{SD}}/f_{\text{WARPS}} = 0.98 \pm 0.26$. We compared our fluxes to those of the SSHARC survey (Burke et al. 2003) and find for the nine shared clusters the mean flux ratio is $f_{160\text{SD}}/f_{\text{SSHARC}} = 0.78 \pm 0.22$. This tendency for the SSHARC fluxes to be somewhat larger than those of the 160SD and other surveys is also noted by Burke et al. (2003).

The statistics concerning the membership of the 160SD clusters in other samples are summarized in Table 5. Six independent cluster surveys, including the 160SD, have been extracted from the same parent dataset, the *ROSAT* archive of pointed PSPC observations. Thus a significant amount of shared objects is anticipated and is confirmed. Given the large solid angle and deep flux limit of our survey, the 201 clusters of 160SD comprise the largest sample

derived from the PSPC archive and encompass approximately 30%–60% of the clusters from similar surveys. By number the largest overlap is 46 clusters shared with the RDCS, whereas by percentage the largest coincidence is the 58% of RIXOS clusters. Not surprisingly there are much fewer matches between the 160SD catalog and the surveys based on the RASS. The 160 deg² sky coverage of our survey is a very small fraction of the near all-sky coverage of the RASS. Furthermore, these RASS-based surveys are largely dominated by nearby ($z \lesssim 0.3$) bright clusters, which were often the target of PSPC observations and thus excluded by design from the 160SD sample. Finally, there are only minor duplications between the *ROSAT* PSPC and the *ROSAT* HRI or *Einstein* IPC pointings, hence the overlaps with the EMSS and BMW-HRI samples are small.

Since the 160SD cluster sample was the first of the *ROSAT* surveys to be published (V98), subsequent groups have had the opportunity to make detailed comparisons to our sample (e.g., BSHARC: Romer et al. 2000; SSHARC: Burke et al. 2003; WARPS-I: Perlman et al. 2002). In each case the authors have made a field-by-field evaluation of their X-ray source detections and cluster identifications versus ours for the *ROSAT* pointings common to both surveys. We highlight and further develop the key results using the revised 160SD catalog.

There are 201 *ROSAT* PSPC fields processed by both the BSHARC and 160SD surveys (Romer et al. 2000, see their § 7.5). Note the BSHARC survey adopted a wide and shallow strategy covering approximately 178 deg² above a flux limit of $\sim 3 \times 10^{-13}$ erg s⁻¹. In the shared area there are twenty-one 160SD clusters which are sufficiently bright as to appear in the BSHARC survey. Thirteen of these X-ray sources are recovered in the BSHARC sample, whereas eight are missing. Six clusters (#9, #42, #107, #182, #195, and #207) were not included because of a failure to meet a filling factor criterion, and two (#110 and #201) were missed because they were not detected as extended (Romer et al. 2000; K. Romer, priv. comm.). The BSHARC filling factor diagnostic was used to reject blends or “percolation runaways”; see Perlman et al. (2002) for a discussion on the impact of this filter on survey completeness. For the thirteen sources successfully detected by the BSHARC survey, we note only two deviations in the optical identifications. First, RX J0947.7+0741 (#75) is identified as a QSO at $z = 0.63$, but we have measured concordant galaxy redshifts at $z = 0.625$ thus suggesting that the extended X-ray emission is the result of the ICM. The QSO was in fact identified as a separate point source by our X-ray analysis software. Second as previously discussed in § 2.3, RX J1524.6+0957 (#170) is listed as a group at $z = 0.078$ whereas we conclude that a $z = 0.516$ cluster is the dominant source. Romer et al. (2000) did not identify any additional clusters within 160SD survey boundaries which are not already part of the 160SD catalog.

Recently Burke et al. (2003, see latter portions of their § 3.1 and § 4) described the results of the SSHARC project and examined the areas of the sky jointly surveyed by both the SSHARC and 160SD. Note that both surveys probe to similar lower flux limits ($\sim 4 \times 10^{-14}$ erg cm⁻² s⁻¹) but the SSHARC was limited to a relatively small solid angle

of 17.7 deg². There are sixteen 160SD clusters in the overlap region. Nine of these are identified as clusters in the SSHARC sample whereas seven are missing. One 160SD cluster (#215), which is also a part of the RDCS sample, was not detected in the SSHARC survey. The remaining six (#39, #43, #75, #83, #124, and #214) were flagged as extended X-ray sources by Burke et al. (2003); however they concluded that their optical follow-up does not suggest the existence of a cluster in any of these cases. Nonetheless, we have measured multiple concordant redshifts for each of these six clusters. Also note clusters #83 and #124 are confirmed members of the WARPS-II and RDCS samples, respectively. Burke et al. (2003) point out one SSHARC cluster (RX J0505.3-2849, $z = 0.509$) which should formally meet our selection criteria but was not included in our catalog because it was detected as two separate sources. We manually inspected the processed *ROSAT* fields during survey construction and suspected this double source was an incorrect result of the X-ray detection algorithm. However, no other similar cases were found in the entire survey, and we opted not to modify the detection software for the sake of this single relatively X-ray faint cluster.

The first phase of the WARPS survey (Perlman et al. 2002, and references therein) is similar in sky coverage to the SSHARC. WARPS-I covered 16.2 deg² down to a flux limit of 6.5×10^{-14} erg s⁻¹ in total flux. The ongoing second phase, WARPS-II, extends the survey area to about 73 deg² (H. Ebeling, priv. comm.). Perlman et al. (2002) scrutinized the 20 *ROSAT* PSPC fields included in both the 160SD and WARPS-I surveys. They found that the 16 cluster identifications in the overlap region are in complete agreement. Furthermore, we note excellent accord in the cluster redshifts except in one case. For RX J0210.4-3929 (#25) we measured a redshift for the BCG of $z = 0.165$ and obtained a low signal-to-noise spectrum of a second galaxy that is consistent with the BCG redshift. In the WARPS-I catalog (Perlman et al. 2002) the redshift is quoted as $z = 0.273$ but is noted to be uncertain. In light of our new evidence the WARPS team re-examined their low-quality spectra for this cluster and find their data are consistent with the 160SD redshift (E. Perlman, priv. comm.).

Finally, we emphasize a very important conclusion that can be drawn from the careful work of the WARPS program. Their survey is unique amongst the complement of cluster searches based upon the *ROSAT* PSPC archive of pointed observations in that they pursued optical identifications for extended X-ray sources as well as for *non*-extended sources. The others, including the 160SD survey, only examined X-ray emitters which were significantly extended. The fact that the WARPS team found no clusters missed by the 160SD, and in particular, no cluster was missed because it was not resolved as extended, underscores the completeness of our survey strategy.

5. SUMMARY

We present the revised catalog of 201 galaxy clusters for the 160SD survey featuring spectroscopic redshifts for 99.5% of the members. This sample includes 30%–60% of the clusters from similar *ROSAT* cluster surveys, and is currently the largest high-redshift sample of X-ray se-

lect clusters in the public domain. We review the X-ray criteria used to locate these galaxy systems, describe the optical imaging and spectroscopy used to classify them, and compare our results with similar studies.

It is a pleasure to thank Piero Rosati, Hans Böhringer, Harald Ebeling, Kathy Romer, Eric Perlman, Stefano Ettori and Axel Schwope for fruitful discussions. We are grateful to Harald Ebeling and the WARPS team, Piero Rosati and the RDCS team, and John Huchra for sharing cluster redshifts prior to publication (respectively 3, 1, and 2 entries referenced in Table 4). Kathy Romer and the BSHARC team kindly shared galaxy redshifts for the foreground group associated with RXJ1524.6+0957. We thank Piero Rosati and the RDCS team for providing the unpublished RDCS sample, and Laurence Jones and the WARPS team for providing access to the unpublished WARPS-II sample to permit cross-correlations with the 160SD clusters. Similarly we appreciate Luigi Guzzo and the BMW-HRI team for sharing the target list for their on-going survey for comparison with the 160SD. Hans Böhringer kindly provided the cross correlation of the un-

published REFLEX-I/II samples and the 160SD clusters. The referee is thanked for providing comments that helped clarify the presentation of this work. The support of the time allocation committees at UH and ESO, and the expertise of the dedicated personnel at the Mauna Kea and La Silla observatories are gratefully acknowledged. The authors recognize the religious and cultural significance of the summit of Mauna Kea to the indigenous people of Hawai'i. We deeply appreciate the opportunity to pursue scientific research from this special place.

C.R.M. acknowledges partial financial support from NASA grant NGT5-50175, the ESO Office for Science, and the ARCS Foundation. The contributions of B.R.M., A.V., W.R.F., and C.J.F. were possible thanks in part to NASA grant NAG5-9217 and contract NAS8-39073. HQ was partially supported by FONDAP Centro de Astrofísica. This research has made use of the NASA/IPAC Extragalactic Database (NED) which is operated by the Jet Propulsion Laboratory, California Institute of Technology, under contract with the National Aeronautics and Space Administration.

REFERENCES

- Abell, G. O., Corwin, H. G., & Olowin, R. P. 1989, *ApJS*, 70, 1
- Allen, S. W., Ettori, S., & Fabian, A. C. 2001, *MNRAS*, 324, 877
- Böhringer, H., Schuecker, P., Guzzo, L., Collins, C. A., Voges, W., Schindler, S., Neumann, D. M., Cruddace, R. G., De Grandi, S., Chincarini, G., Edge, A. C., MacGillivray, H. T., & Shaver, P. 2001, *A&A*, 369, 826
- Böhringer, H., Voges, W., Huchra, J. P., McLean, B., Giacconi, R., Rosati, P., Burg, R., Mader, J., Schuecker, P., Simic, D., Komossa, S., Reiprich, T. H., Retzlaff, J., & Trümper, J. 2000, *ApJS*, 129, 435
- Bond, J. R., Kofman, L., & Pogosyan, D. 1996, *Nature*, 380, 603
- Borgani, S. & Guzzo, L. 2001, *Nature*, 409, 39
- Borgani, S., Rosati, P., Tozzi, P., Stanfod, S. A., Eisenhardt, P. R., Lidman, C., Holden, B., Della Ceca, R., Norman, C., & Squires, G. 2001, *ApJ*, 561, 13
- Boyle, B. J., Wilkes, B. J., & Elvis, M. 1997, *MNRAS*, 285, 511
- Burke, D. J., Collins, C. A., Sharples, R. M., Romer, A. K., & Nichol, R. C. 2003, *MNRAS*, accepted
- Carlstrom, J. E., Holder, G. P., & Reese, E. D. 2002, *ARA&A*, 40, 643
- Castander, F. J., Bower, R. G., Ellis, R. S., Aragon-Salamanca, A., Mason, K. O., Hasinger, G., McMahon, R. G., Carrera, F. J., Mittaz, J. P. D., Perez-Fournon, I., & Lehto, H. J. 1995, *Nature*, 377, 39
- Cavaliere, A. & Fusco-Femiano, R. 1976, *A&A*, 49, 137
- Clowe, D. & Schneider, P. 2002, *A&A*, 395, 385
- Couch, W. J., Ellis, R. S., MacLaren, I., & Malin, D. F. 1991, *MNRAS*, 249, 606
- Cruddace, R., Voges, W., Böhringer, H., Collins, C. A., Romer, A. K., MacGillivray, H., Yentis, D., Schuecker, P., Ebeling, H., & De Grandi, S. 2002, *ApJS*, 140, 239
- . 2003, *ApJS*, 144, 299
- Czoske, O., Moore, B., Kneib, J.-P., & Soucail, G. 2002, *A&A*, 386, 31
- De Grandi, S., Böhringer, H., Guzzo, L., Molendi, S., Chincarini, G., Collins, C., Cruddace, R., Neumann, D., Schindler, S., Schuecker, P., & Voges, W. 1999, *ApJ*, 514, 148
- Donahue, M., Mack, J., Scharf, C., Lee, P., Postman, M., Rosati, P., Dickinson, M., Voit, G. M., & Stocke, J. T. 2001, *ApJ*, 552, L93
- Donahue, M., Scharf, C. A., Mack, J., Lee, Y. P., Postman, M., Rosati, P., Dickinson, M., Voit, G. M., & Stocke, J. T. 2002, *ApJ*, 569, 689
- Ebeling, H., Edge, A. C., Allen, S. W., Crawford, C. S., Fabian, A. C., & Huchra, J. P. 2000, *MNRAS*, 318, 333
- Ebeling, H., Edge, A. C., Böhringer, H., Allen, S. W., Crawford, C. S., Fabian, A. C., Voges, W., & Huchra, J. P. 1998, *MNRAS*, 301, 881
- Ebeling, H., Edge, A. C., & Henry, J. P. 2001, *ApJ*, 553, 668
- Ebeling, H., Mullis, C. R., & Tully, R. B. 2002, *ApJ*, 580, 774
- Gioia, I. M., Henry, J. P., Maccacaro, T., Morris, S. L., Stocke, J. T., & Wolter, A. 1990, *ApJ*, 356, L35
- Gioia, I. M., Henry, J. P., Mullis, C. R., Ebeling, H., & Wolter, A. 1999, *AJ*, 117, 2608
- Gioia, I. M., Henry, J. P., Mullis, C. R., Voges, W., Briel, U. G., Böhringer, H., & Huchra, J. P. 2003, *ApJS*, submitted
- Gioia, I. M. & Luppino, G. A. 1994, *ApJS*, 94, 583
- Griffiths, R. E., Tuohy, I. R., Brissenden, R. J. V., & Ward, M. J. 1992, *MNRAS*, 255, 545
- Henry, J. P. 2000, *ApJ*, 534, 565
- Henry, J. P., Gioia, I. M., Maccacaro, T., Morris, S. L., Stocke, J. T., & Wolter, A. 1992, *ApJ*, 386, 408
- Henry, J. P., Gioia, I. M., Mullis, C. R., Voges, W., Briel, U. G., Böhringer, H., & Huchra, J. P. 2001, *ApJ*, 553, L109
- Hornstrup, A., McNamara, B. R., Vikhlinin, A., Greve, T. R., Forman, W. R., & Jones, C. 2003, *ApJ*, submitted
- Huchra, J. P., Geller, M. J., Henry, J. P., & Postman, M. 1990, *ApJ*, 365, 66
- Huchra, J. P., Vogeley, M. S., & Geller, M. J. 1999, *ApJS*, 121, 287
- Jenkins, A., Frenk, C. S., Pearce, F. R., Thomas, P. A., Colberg, J. M., White, S. D. M., Couchman, H. M. P., Peacock, J. A., Efstathiou, G., & Nelson, A. H. 1998, *ApJ*, 499, 20
- Jones, C. & Forman, W. 1999, *ApJ*, 511, 65
- Jones, L. R., Ponman, T. J., & Forbes, D. A. 2000, *MNRAS*, 312, 139
- Kopylov, A. I., Fetisova, T. S., & Shvartsman, V. F. 1984, *Astronomicheskij Tsirkulyar*, 1344, 1
- Kurtz, M. J., Huchra, J. P., Beers, T. C., Geller, M. J., Gioia, I. M., Maccacaro, T., Schild, R. E., & Stauffer, J. R. 1985, *AJ*, 90, 1665
- Loveday, J., Peterson, B. A., Maddox, S. J., & Efstathiou, G. 1996, *ApJS*, 107, 201
- Mahdavi, A., Böhringer, H., Geller, M. J., & Ramella, M. 2000, *ApJ*, 534, 114
- Markevitch, M., Gonzalez, A. H., David, L., Vikhlinin, A., Murray, S., Forman, W., Jones, C., & Tucker, W. 2002, *ApJ*, 567, L27
- Mason, K. O., Carrera, F. J., Hasinger, G., Andernach, H., Aragon-Salamanca, A., Barcons, X., Bower, R., Brandt, W. N., Branduardi-Raymont, G., Burgos-Martín, J., Cabrera-Guerra, F., Carballo, R., Castander, F., Ellis, R. S., González-Serrano, J. I., Martínez-González, E., Martín-Mirones, J. M., McMahon, R. G., Mittaz, J. P. D., Nicholson, K. L., Page, M. J., Pérez-Fournon, I., Puchnarewicz, E. M., Romero-Colmenero, E., Schwope, A. D., Vila, B., Watson, M. G., & Wonnacott, D. 2000, *MNRAS*, 311, 456
- Massey, P., Strobel, K., Barnes, J. V., & Anderson, E. 1988, *ApJ*, 328, 315
- McHardy, I. M., Jones, L. R., Merrifield, M. R., Mason, K. O., Newsam, A. M., Abraham, R. G., Dalton, G. B., Carrera, F., Smith, P. J., Rowan-Robinson, M., & Abraham, R. G. 1998, *MNRAS*, 295, 641
- McNamara, B. R., Vikhlinin, A., Hornstrup, A., Quintana, H., Whitman, K., Forman, W., & Jones, C. 2001, *ApJ*, 558, 590

- Moretti, A., Guzzo, L., Campana, S., Covino, S., Lazzati, D., Longhetti, M., Molinari, E., Panzera, M. R., Tagliaferri, G., & dell'Antonio, I. 2001, in ASP Conf. Ser. 234: X-ray Astronomy 2000, 393
- Muñoz, J. A., Falco, E. E., Kochanek, C. S., Lehár, J., McLeod, B. A., McNamara, B. R., Vikhlinin, A. A., Impey, C. D., Rix, H., Keeton, C. R., Peng, C. Y., & Mullis, C. R. 2001, ApJ, 546, 769
- Mulchaey, J. S. 2000, ARA&A, 38, 289
- Mullis, C. R. 2001, Ph.D. Thesis, Univ. of Hawaii
- Mullis, C. R., Henry, J. P., Gioia, I. M., Böhringer, H., Briel, U. G., Voges, W., & Huchra, J. P. 2001, ApJ, 553, L115
- Mullis, C. R., Vikhlinin, A., Henry, J. P., McNamara, B. R., Quintana, H., Gioia, I. M., Hornstrup, A., Way, M., Forman, W., & Jones, C. 2003, in preparation
- Nesci, R. & Altamore, A. 1990, A&A, 234, 60
- Oegerle, W. R., Hill, J. M., & Fitchett, M. J. 1995, AJ, 110, 32+
- Oke, J. B., Cohen, J. G., Carr, M., Cromer, J., Dingizian, A., Harris, F. H., Labrecque, S., Lucinio, R., Schaal, W., Epps, H., & Miller, J. 1995, PASP, 107, 375
- Oke, J. B. & Gunn, J. E. 1983, ApJ, 266, 713
- Panzera, M. R., Campana, S., Covino, S., Lazzati, D., Mignani, R. P., Moretti, A., & Tagliaferri, G. 2003, A&A, 399, 351
- Peacock, J. A. 1999, Cosmological Physics (Cambridge, UK: Cambridge University Press)
- Peebles, P. J. E. 1993, Principles of Physical Cosmology (Princeton, NJ: Princeton University Press)
- Perlman, E. S., Horner, D. J., Jones, L. R., Scharf, C. A., Ebeling, H., Wegner, G., & Malkan, M. 2002, ApJS, 140, 265
- Ponman, T. J., Allan, D. J., Jones, L. R., Merrifield, M., McHardy, I. M., Lehto, H. J., & Luppino, G. A. 1994, Nature, 369, 462
- Postman, M. 2002, in ASP Conf. Ser. TBD: Tracing Cosmic Evolution with Galaxy Clusters, 1
- Quintana, H. & Ramirez, A. 1995, ApJS, 96, 343
- Raymond, J. C. & Smith, B. W. 1977, ApJS, 35, 419
- Romer, A. K., Nichol, R. C., Holden, B. P., Ulmer, M. P., Pildis, R. A., Merrelli, A. J., Adami, C., Burke, D. J., Collins, C. A., Metevier, A. J., Kron, R. G., & Commons, K. 2000, ApJS, 126, 209
- Rosati, P., Borgani, S., & Norman, C. 2002, ARA&A, 40, 539
- Rosati, P., della Ceca, R., Burg, R., Norman, C., & Giacconi, R. 1995, ApJ, 445, L11
- Rosati, P., della Ceca, R., Norman, C., & Giacconi, R. 1998, ApJ, 492, L21
- Rosati, P., Stanford, S. A., Eisenhardt, P. R., Elston, R., Spinrad, H., Stern, D., & Dey, A. 1999, AJ, 118, 76
- Rose, J. A., Gaba, A. E., Christiansen, W. A., Davis, D. S., Caldwell, N., Hunstead, R. W., & Johnston-Hollitt, M. 2002, AJ, 123, 1216
- Sarazin, C. L. 1988, X-ray emission from clusters of galaxies (Cambridge Astrophysics Series, Cambridge: Cambridge University Press)
- Scharf, C. A., Jones, L. R., Ebeling, H., Perlman, E., Malkan, M., & Wegner, G. 1997, ApJ, 477, 79
- Schmidt, M., Hasinger, G., Gunn, J., Schneider, D., Burg, R., Giacconi, R., Lehmann, I., MacKenty, J., Trümper, J., & Zamorani, G. 1998, A&A, 329, 495
- Schneider, D. P., Gunn, J. E., & Hoessel, J. G. 1983, ApJ, 264, 337
- Schwope, A., Hasinger, G., Lehmann, I., Schwarz, R., Brunner, H., Neizvestny, S., Ugryumov, A., Balega, Y., Trümper, J., & Voges, W. 2000, AN, 321, 1
- Silk, J. & White, S. D. M. 1978, ApJ, 226, L103
- Smail, I., Ellis, R. S., Dressler, A., Couch, W. J., Oemler, A. J., Sharples, R. M., & Butcher, H. 1997, ApJ, 479, 70
- Stanford, S. A., Holden, B., Rosati, P., Tozzi, P., Borgani, S., Eisenhardt, P. R., & Spinrad, H. 2001, ApJ, 552, 504
- Stocke, J. T., Morris, S. L., Gioia, I. M., Maccacaro, T., Schild, R., Wolter, A., Fleming, T. A., & Henry, J. P. 1991, ApJS, 76, 813
- Struble, M. F. & Rood, H. J. 1999, ApJS, 125, 35
- Sunyaev, R. A. & Zeldovich, Y. B. 1972, Com.Ap, 4, 173
- Trümper, J. 1993, Science, 260, 1769
- Ulrich, M.-H. 1976, ApJ, 206, 364
- Vikhlinin, A., Markevitch, M., & Murray, S. S. 2001, ApJ, 551, 160
- Vikhlinin, A., McNamara, B. R., Forman, W., Jones, C., Quintana, H., & Hornstrup, A. 1998a, ApJ, 502, 558
- . 1998b, ApJ, 498, L21
- Vikhlinin, A., McNamara, B. R., Hornstrup, A., Quintana, H., Forman, W., Jones, C., & Way, M. 1999, ApJ, 520, L1
- Vikhlinin, A., VanSpeybroeck, L., Markevitch, M., Forman, W. R., & Grego, L. 2002, ApJ, 578, L107
- Vikhlinin, A., Voevodkin, A., Mullis, C., VanSpeybroeck, L., Quintana, H., McNamara, B., Gioia, I., Hornstrup, A., Henry, J., Forman, W., & Jones, J. 2003, ApJ, submitted, 1, 1
- Voges, W. 1992, Proceedings of Satellite Symposium 3, EAS ISY-3, 9
- Weinberg, S. 1972, Gravitation and Cosmology: Principles and Applications of the General Theory of Relativity (New York: John Wiley & Sons)
- White, D. A., Jones, C., & Forman, W. 1997, MNRAS, 292, 419
- Wu, X., Chiueh, T., Fang, L., & Xue, Y. 1998, MNRAS, 301, 861

TABLE 1

X-RAY SELECTED CLUSTER SURVEYS

| Acronym | Name | Reference |
|----------|---|--|
| 160SD | 160 Square Degree <i>ROSAT</i> Cluster Survey | Vikhlinin et al. 1998a; this paper |
| BCS+eBCS | Brightest Cluster Sample + Extended Brightest Cluster Sample | Ebeling et al. 1998, 2000 |
| BMW-HRI | Brera Multiscale Wavelet <i>ROSAT</i> HRI Cluster Survey | Moretti et al. 2001; Panzera et al. 2003 |
| BSHARC | Bright Serendipitous High-Redshift Archival <i>ROSAT</i> Cluster Survey | Romer et al. 2000 |
| CIZA | Clusters in the Zone of Avoidance Survey | Ebeling, Mullis, & Tully 2002 |
| EMSS | <i>Einstein</i> Extended Medium Sensitivity Survey | Gioia et al. 1990; Henry et al. 1992 |
| MACS | Massive Cluster Survey | Ebeling, Edge, & Henry 2001 |
| NEP | <i>ROSAT</i> North Ecliptic Pole Survey | Henry et al. 2001; Mullis 2001 |
| NORAS | Northern <i>ROSAT</i> All-Sky Galaxy Cluster Survey | Böhringer et al. 2000 |
| RASS1BS | RASS1 Bright Sample | De Grandi et al. 1999 |
| RDCS | <i>ROSAT</i> Distant Cluster Survey | Rosati et al. 1995, 1998 |
| REFLEX | <i>ROSAT</i> -ESO Flux Limited X-ray Galaxy Cluster Survey | Böhringer et al. 2001 |
| RIXOS | <i>ROSAT</i> International X-ray/Optical Survey | Castander et al. 1995; Mason et al. 2000 |
| RBS | <i>ROSAT</i> Bright Survey | Schwope et al. 2000 |
| ROXS | <i>ROSAT</i> Optical X-Ray Survey | Donahue et al. 2001, 2002 |
| SGP | <i>ROSAT</i> South Galactic Pole Survey | Craddock et al. 2002, 2003 |
| SSHARC | Southern Serendipitous High-Redshift Archival <i>ROSAT</i> Cluster Survey | Burke et al. 2003 |
| WARPS | Wide Angle <i>ROSAT</i> Pointed Survey | Scharf et al. 1997; Perlman et al. 2002 |

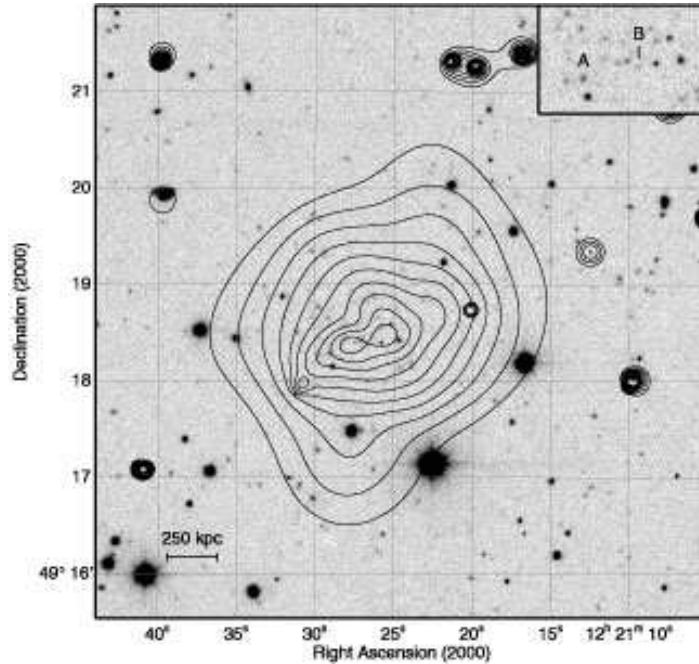


FIG. 1.— RX J1221.4+4918 (#119): a distant cluster at $z = 0.700$. A 5 minute R -band image taken with the FLWO 1.2m on 25 Jan 1998 is overlaid with adaptively smoothed X-ray flux contours in the 0.7–2.0 keV band from an 80 ks observation with the *Chandra* ACIS-I. Contours are logarithmically spaced by factors of 1.4 with the lowest contour a factor of 2 above the background (5.5×10^{-4} counts s^{-1} arcmin²). Features in the X-ray contours are significant at a level of $\geq 4\sigma$. The inset (upper-right) indicates the cluster galaxies for which redshifts were measured (see spectra in Figure 2). The R -band magnitude of galaxy A is 20.23. The scale bar shows the angular size of 250 kpc at $z = 0.700$.

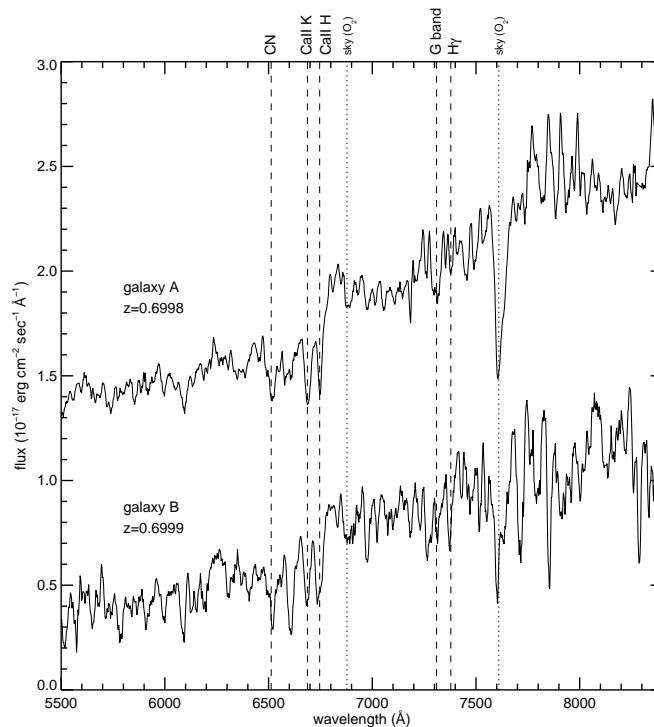


FIG. 2.— RX J1221.4+4918 (#119): a distant cluster at $z = 0.700$. Longslit spectra of galaxies A and B measured with Keck-II LRIS on 08 Jul 1999. Total integration time was 30 minutes. Galaxy A is vertically displaced by 1×10^{-17} and galaxy B is scaled by a factor of 2 for an optimal comparison of the spectra. The measured redshifts are $z_A = 0.6998 \pm 0.0004$ and $z_B = 0.6999 \pm 0.0008$. The dashed lines indicate the positions of stellar absorption features at the cluster redshift ($z = 0.700$) and the dotted lines mark the wavelengths of atmospheric absorption bands.

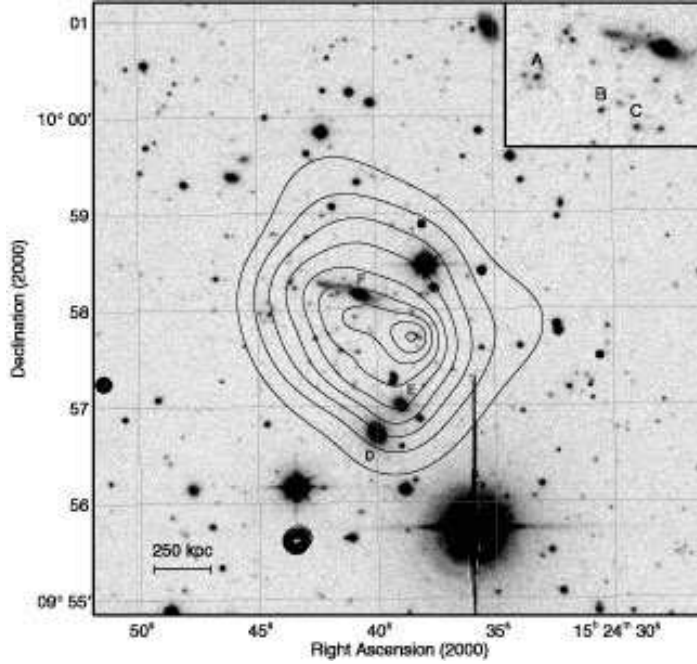


FIG. 3.— RX J1524.6+0957 (#170): a nearby group ($z = 0.078$) and a distant cluster ($z = 0.516$). A 10 minute I -band image taken with the FLWO 1.2m on 08 Jul 1997 is overlaid with adaptively smoothed X-ray flux contours in the 0.7–2.0 keV band from a 51 ks observation with the *Chandra* ACIS-I. Contours are logarithmically spaced by factors of 1.4 with the lowest contour a factor of 2 above the background (9.7×10^{-4} counts s^{-1} arcmin 2). Features in the X-ray contours are significant at a level of $\gtrsim 4\sigma$. The inset (upper-right) indicates the galaxies (A–C) of the distant cluster for which redshifts were measured (see spectra in Figure 4). The foreground group galaxies (D–F) are at redshifts $z_D = 0.0787 \pm 0.0009$, $z_E = 0.0767 \pm 0.0009$, and $z_F = 0.08?$ (K. Romer, priv. comm.). The R -band magnitude of galaxy C is 20.29. The scale bar shows the angular size of 250 kpc at $z = 0.516$.

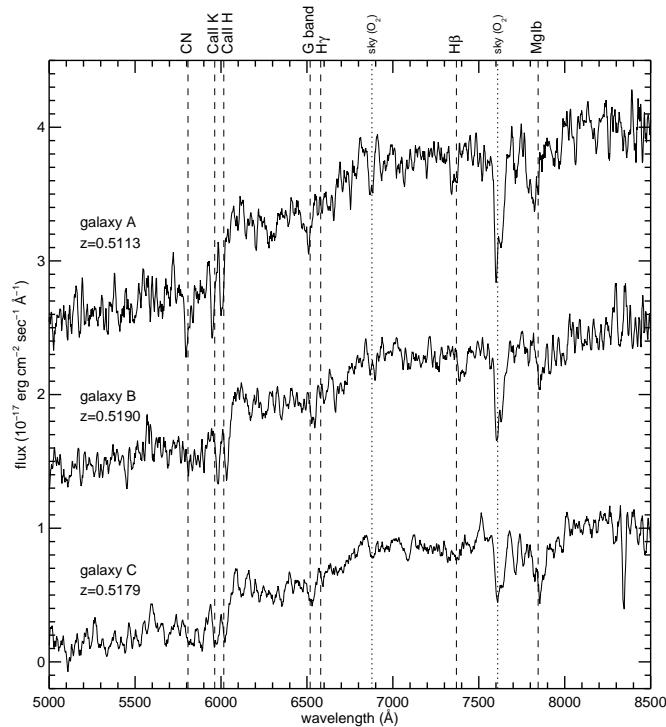


FIG. 4.— RX J1524.6+0957 (#170): a nearby group ($z = 0.078$) and a distant cluster ($z = 0.516$). Longslit spectra of galaxies A, B, and C measured with Keck-II LRIS on 27 Jan 2000. Total integration time was 20 minutes. Galaxies A and B are vertically displaced by 2×10^{-17} and 1×10^{-17} , respectively, for an optimal comparison of the spectra. The measured redshifts are $z_A = 0.5113 \pm 0.0002$, $z_B = 0.5190 \pm 0.0005$ and $z_C = 0.5179 \pm 0.0004$. The dashed lines indicate the positions of stellar absorption features at the cluster redshift ($z = 0.516$) and the dotted lines mark the wavelengths of atmospheric absorption bands.

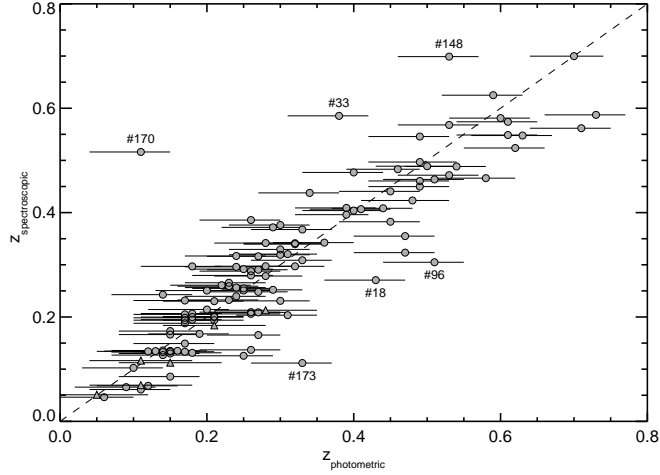


FIG. 5.— Spectroscopic redshift versus photometric redshift for the 124 clusters of the 160SD sample originally published with photometric redshifts in V98. The circles represent the 117 objects for which the photometric redshift estimates were based on CCD imaging; whereas the triangles represent the 7 objects for which photometric redshifts were based on DSS images. The horizontal error bars are the 90% confidence intervals for the photometric redshift estimates. The errors on the spectroscopic measurements are smaller than the plotting symbols. The six clusters with the largest redshift difference are labeled.

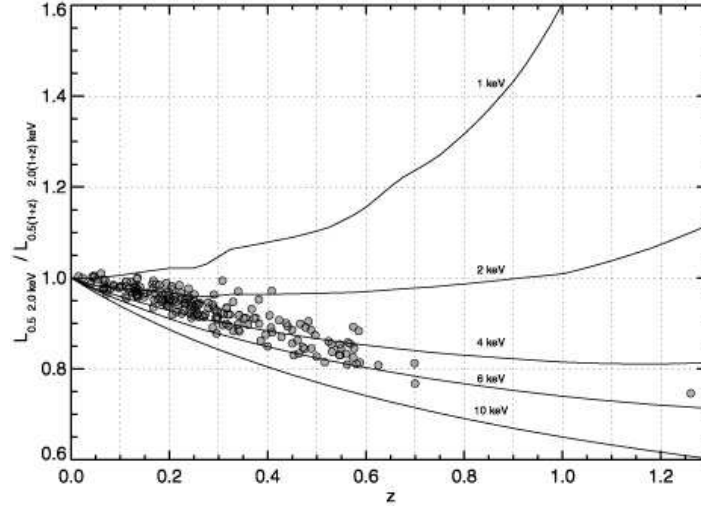


FIG. 6.— K -corrections as a function of redshift and ICM temperature in the 0.5 – 2.0 keV band. The model source spectrum is a Raymond-Smith plasma with a metallicity of 0.3 solar. Data points indicate the sampling of the 160SD clusters. The trend of increasing cluster temperature with increasing redshift is the result of the flux-limited nature of the survey.

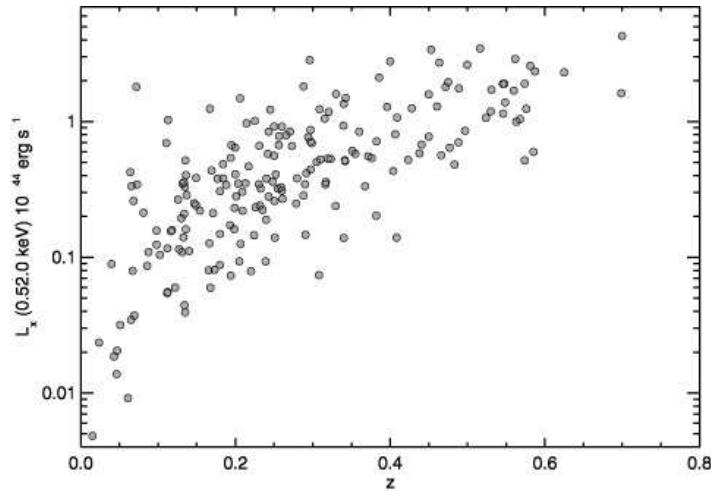


FIG. 7.— X-ray luminosity and redshift distribution of the 160SD cluster sample. The median redshift is $z_{\text{median}} = 0.25$ and the median X-ray luminosity is $L_{X,\text{median}} = 4.2 \times 10^{43} \text{ erg s}^{-1}$. To preserve the readability of this plot the most distant cluster (RX J0848.9+4452, $z = 1.261$, $L_X = 2.0 \times 10^{44} \text{ erg s}^{-1}$) is not shown.

TABLE 2
OPTICAL IDENTIFICATIONS OF 160SD X-RAY SOURCES

| | V98 | Revised Sample (this work) |
|--|-----|-------------------------------|
| extended X-ray sources | 223 | 223 |
| galaxy clusters | 203 | 201 |
| probable false detections ^a | 19 | 21 |
| no follow-up observations ^b | 1 | 1 |

^alikely blends of unresolved X-ray point sources

^bobscured by the glare of Arcturus

TABLE 3
REDSHIFTS FOR 160SD CLUSTERS

| | V98 | Newly Reported (this work) | Revised Sample (this work) |
|----------------------------|-----|-------------------------------|-------------------------------|
| spectroscopic redshifts | 76 | 124 | 200 |
| measured by our group | 45 | 110 | 155 |
| literature & private comm. | 31 | 14 | 45 |
| photometric estimates | 124 | ... | ... |
| clusters with no redshift | 3 | ... | 1 |
| cluster sample size | 203 | ... | 201 |

TABLE 4
160 SQUARE DEGREE *ROSAT* SURVEY CLUSTER CATALOG

| Object Name | Number | α [J2000] (3) | δ [J2000] (4) | δr [$''$] (5) | r_c [$''$] (6) | δr_c [$''$] (7) | f_X [10^{-14} cgs] (8) | δf_X [10^{-14} cgs] (9) | L_X [10^{44} cgs] (10) | z (11) | Redshift References (12) | Notes (13) |
|-----------------|--------|----------------------------|----------------------------|-------------------------------|--------------------------|---------------------------------|-----------------------------------|--|-----------------------------------|-------------|--------------------------------|----------------------------------|
| RX J0030.5+2618 | 1 | 00 30 33.2 | +26 18 19 | 13 | 31 | 3 | 24.3 | 3.0 | 2.61 | 0.500 | | RDCS/WARPS2 |
| RX J0041.1-2339 | 2 | 00 41 10.3 | -23 39 33 | 19 | 25 | 12 | 9.8 | 2.4 | 0.06 | 0.112 | | |
| RX J0050.9-0929 | 3 | 00 50 59.2 | -09 29 12 | 11 | 45 | 4 | 36.6 | 4.9 | 0.64 | 0.200 | | WARPS2 |
| RX J0054.0-2823 | 4 | 00 54 02.8 | -28 23 58 | 16 | 37 | 6 | 10.8 | 1.5 | 0.42 | 0.292 | | RDCS/WARP2 |
| RX J0056.9-2213 | 5 | 00 56 55.8 | -22 13 53 | 17 | 61 | 12 | 25.9 | 5.2 | 0.16 | 0.116 | | |
| RX J0056.9-2740 | 6 | 00 56 56.1 | -27 40 12 | 13 | 14 | 2 | 6.9 | 0.8 | 1.00 | 0.563 | 1 | J1888.16, RDCS |
| RX J0057.4-2616 | 7 | 00 57 24.2 | -26 16 45 | 14 | 82 | 6 | 186.1 | 21.3 | 1.03 | 0.113 | 2 | A122/REFLEX2 |
| RX J0110.3+1938 | 8 | 01 10 18.0 | +19 38 23 | 16 | 35 | 8 | 7.8 | 1.6 | 0.36 | 0.317 | | WARPS2 |
| RX J0111.6-3811 | 9 | 01 11 36.6 | -38 11 12 | 9 | 18 | 3 | 8.9 | 1.7 | 0.06 | 0.122 | | WARPS1 |
| RX J0122.5-2832 | 10 | 01 22 35.9 | -28 32 03 | 14 | 37 | 16 | 26.9 | 6.3 | 0.78 | 0.256 | | Abell S154 |
| RX J0124.5+0400 | 11 | 01 24 35.1 | +04 00 49 | 20 | 31 | 14 | 7.5 | 2.2 | 0.34 | 0.316 | | |
| RX J0127.4-4326 | 12 | 01 27 27.8 | -43 26 13 | 19 | 34 | 13 | 5.7 | 1.9 | F | F | | F |
| RX J0128.6-4324 | 13 | 01 28 36.9 | -43 24 57 | 9 | 10 | 3 | 7.5 | 1.3 | 0.28 | 0.288 | | |
| RX J0132.9-4259 | 14 | 01 32 54.7 | -42 59 52 | 23 | 75 | 25 | 32.3 | 8.1 | 0.11 | 0.088 | 3 | APMBGC 244-064-098 |
| RX J0136.4-1811 | 15 | 01 36 24.2 | -18 11 59 | 15 | 21 | 8 | 4.8 | 1.0 | 0.14 | 0.251 | | WARPS2 |
| RX J0139.6+0119 | 16 | 01 39 39.5 | +01 19 27 | 12 | 37 | 8 | 10.9 | 2.0 | 0.32 | 0.255 | | z_{PSPC} , RDCS/WARPS2 |
| RX J0139.9+1810 | 17 | 01 39 54.3 | +18 10 00 | 9 | 33 | 5 | 27.3 | 3.8 | 0.38 | 0.177 | 2 | A227/RDCS |
| RX J0142.8+2025 | 18 | 01 42 50.6 | +20 25 16 | 22 | 29 | 6 | 26.1 | 4.5 | 0.84 | 0.271 | | BMW |
| RX J0144.4+0212 | 19 | 01 44 29.1 | +02 12 37 | 13 | 32 | 11 | 10.1 | 2.3 | 0.13 | 0.166 | | WARPS1 |
| RX J0154.2-5937 | 20 | 01 54 14.8 | -59 37 48 | 12 | 22 | 7 | 14.5 | 3.2 | 0.84 | 0.360 | | |
| RX J0159.3+0030 | 21 | 01 59 18.2 | +00 30 12 | 9 | 13 | 2 | 32.7 | 4.1 | 2.11 | 0.386 | | |
| RX J0206.3+1511 | 22 | 02 06 23.4 | +15 11 16 | 14 | 53 | 10 | 13.0 | 2.5 | 0.36 | 0.248 | | RDCS/RIXOS/WARPS1 |
| RX J0206.8-1309 | 23 | 02 06 49.5 | -13 09 04 | 15 | 28 | 8 | 26.0 | 4.4 | 1.18 | 0.320 | | |
| RX J0210.2-3932 | 24 | 02 10 13.8 | -39 32 51 | 11 | 22 | 10 | 4.6 | 1.1 | 0.06 | 0.168 | | RDCS |
| RX J0210.4-3929 | 25 | 02 10 25.6 | -39 29 47 | 14 | 28 | 9 | 6.4 | 1.3 | 0.08 | 0.165 | | RDCS/WARPS1 |
| RX J0228.2-1005 | 26 | 02 28 13.2 | -10 05 40 | 15 | 35 | 6 | 24.4 | 3.9 | 0.24 | 0.149 | | WARPS1 |
| RX J0236.0-5225 | 27 | 02 36 05.2 | -52 25 03 | 9 | 16 | 4 | 5.8 | 1.2 | F | F | | F |
| RX J0237.9-5224 | 28 | 02 37 59.2 | -52 24 40 | 14 | 49 | 8 | 64.4 | 8.2 | 0.52 | 0.135 | 4 | A3038/BSHARC/RDCS/REFLEX2/WARPS1 |
| RX J0239.8-2320 | 29 | 02 39 52.6 | -23 20 35 | 23 | 51 | 14 | 8.4 | 1.8 | 0.77 | 0.450 | | |
| RX J0258.7+0012 | 30 | 02 58 46.1 | +00 12 44 | 19 | 28 | 7 | 10.8 | 2.9 | 0.33 | 0.259 | | |
| RX J0259.5+0013 | 31 | 02 59 33.9 | +00 13 47 | 12 | 42 | 11 | 32.4 | 5.2 | 0.54 | 0.194 | | |
| RX J0322.3-4918 | 32 | 03 22 20.1 | -49 18 40 | 15 | 69 | 11 | 40.3 | 7.2 | 0.08 | 0.067 | 5 | z_{PSPC} , Abell S34 |
| RX J0337.7-2522 | 33 | 03 37 44.9 | -25 22 39 | 8 | 7 | 2 | 3.7 | 0.7 | 0.60 | 0.585 | | RDCS/SSHARC |
| RX J0341.9-4500 | 34 | 03 41 57.1 | -45 00 11 | 12 | 27 | 9 | 1.7 | 0.4 | 0.14 | 0.408 | | RDCS |
| RX J0351.6-3649 | 35 | 03 51 37.8 | -36 49 50 | 24 | 31 | 17 | 8.8 | 2.2 | 0.56 | 0.372 | | |
| RX J0428.7-3805 | 36 | 04 28 43.0 | -38 05 54 | 20 | 54 | 13 | 20.8 | 5.0 | 0.22 | 0.154 | 5 | A3259 |
| RX J0434.2-0831 | 37 | 04 34 15.7 | -08 31 17 | 24 | 25 | 14 | 7.2 | 2.2 | 0.19 | 0.240 | | |
| RX J0505.9-2825 | 38 | 05 05 57.8 | -28 25 47 | 15 | 25 | 4 | 14.2 | 1.9 | 0.11 | 0.131 | | RDCS/SSHARC |
| RX J0506.0-2840 | 39 | 05 06 03.7 | -28 40 44 | 21 | 84 | 20 | 19.5 | 3.4 | 0.16 | 0.136 | | |
| RX J0521.1-2530 | 40 | 05 21 10.7 | -25 30 44 | 15 | 37 | 13 | 17.6 | 4.0 | 2.57 | 0.581 | | |
| RX J0522.2-3625 | 41 | 05 22 14.2 | -36 25 04 | 9 | 16 | 5 | 18.4 | 3.8 | 1.79 | 0.472 | | BMW |
| RX J0528.6-3251 | 42 | 05 28 40.3 | -32 51 38 | 8 | 26 | 3 | 19.9 | 2.5 | 0.66 | 0.273 | | RDCS/WARPS2 |
| RX J0529.6-5848 | 43 | 05 29 38.4 | -58 48 10 | 9 | 10 | 3 | 5.6 | 1.0 | 0.56 | 0.466 | | |
| RX J0532.7-4614 | 44 | 05 32 43.7 | -46 14 11 | 7 | 12 | 1 | 41.1 | 4.3 | 0.33 | 0.135 | | |
| RX J0533.8-5746 | 45 | 05 33 53.2 | -57 46 52 | 37 | 81 | 28 | 22.2 | 6.1 | 0.87 | 0.297 | | |
| RX J0533.9-5809 | 46 | 05 33 55.9 | -58 09 16 | 30 | 53 | 20 | 9.0 | 2.8 | 0.16 | 0.198 | | |
| RX J0810.3+4216 | 47 | 08 10 23.9 | +42 16 24 | 14 | 59 | 5 | 238.6 | 27.2 | 0.42 | 0.064 | | |
| RX J0818.9+5654 | 48 | 08 18 57.8 | +56 54 34 | 17 | 29 | 9 | 10.1 | 2.5 | 0.31 | 0.260 | | |
| RX J0819.3+7054 | 49 | 08 19 22.6 | +70 54 48 | 15 | 24 | 6 | 10.1 | 1.8 | 0.23 | 0.226 | | WARPS2 |
| RX J0819.9+5634 | 50 | 08 19 54.4 | +56 34 35 | 14 | 16 | 5 | 30.8 | 5.0 | 0.92 | 0.260 | | |
| RX J0820.4+5645 | 51 | 08 20 26.4 | +56 45 22 | 18 | 39 | 14 | 22.9 | 4.2 | 0.02 | 0.043 | | |
| RX J0826.1+2625 | 52 | 08 26 06.4 | +26 25 47 | 22 | 59 | 19 | 10.9 | 2.6 | 0.61 | 0.351 | | |
| RX J0826.4+3125 | 53 | 08 26 29.7 | +31 25 15 | 31 | 47 | 22 | 11.1 | 4.7 | 0.22 | 0.209 | | |
| RX J0831.2+4905 | 54 | 08 31 16.0 | +49 05 06 | 17 | 30 | 15 | 12.3 | 4.0 | F | F | | F |
| RX J0834.4+1933 | 55 | 08 34 27.4 | +19 33 24 | 18 | 31 | 7 | 8.3 | 1.7 | F | F | | F |
| RX J0841.1+6422 | 56 | 08 41 07.4 | +64 22 43 | 8 | 35 | 3 | 29.1 | 3.2 | 1.49 | 0.342 | | RDCS |
| RX J0841.7+7046 | 57 | 08 41 43.4 | +70 46 53 | 13 | 31 | 12 | 8.9 | 2.1 | 0.22 | 0.235 | | |
| RX J0842.8+5023 | 58 | 08 42 52.8 | +50 23 16 | 16 | 23 | 10 | 6.3 | 1.7 | 0.52 | 0.423 | | |
| RX J0847.1+3449 | 59 | 08 47 11.3 | +34 49 16 | 17 | 28 | 9 | 12.2 | 3.0 | 1.69 | 0.560 | | |

TABLE 4—Continued

| Object Name | Number | α [J2000] (3) | δ [J2000] (4) | δr ["] (5) | r_c ["] (6) | δr_c ["] (7) | f_X [10^{-14} cgs] (8) | δf_X [10^{-14} cgs] (9) | L_X [10^{44} cgs] (10) | z (11) | Redshift References (12) | Notes (13) |
|-----------------|--------|----------------------------|----------------------------|--------------------------|---------------------|----------------------------|-----------------------------------|--|-----------------------------------|-------------|--------------------------------|--|
| (1) | (2) | (3) | (4) | (5) | (6) | (7) | (8) | (9) | (10) | (11) | (12) | (13) |
| RX J0848.7+4456 | 60 | 08 48 47.6 | +44 56 21 | 13 | 14 | 4 | 3.3 | 0.6 | 0.52 | 0.574 | | RDCS/WARPS2 |
| RX J0848.9+4452 | 61 | 08 48 56.3 | +44 52 16 | 14 | 23 | 6 | 2.7 | 0.6 | 1.99 | 1.261 | 6 | RDCS |
| RX J0849.1+3731 | 62 | 08 49 11.1 | +37 31 25 | 14 | 36 | 10 | 14.7 | 3.0 | 0.38 | 0.240 | | BSHARC/RIXOS/WARPS2 |
| RX J0852.5+1618 | 63 | 08 52 33.6 | +16 18 08 | 19 | 33 | 10 | 37.1 | 6.2 | 0.16 | 0.098 | | |
| RX J0853.2+5759 | 64 | 08 53 14.1 | +57 59 39 | 17 | 35 | 14 | 19.8 | 5.8 | 1.95 | 0.475 | | |
| RX J0857.7+2747 | 65 | 08 57 45.7 | +27 47 32 | 27 | 42 | 11 | 6.8 | 1.6 | F | F | | F |
| RX J0858.4+1357 | 66 | 08 58 25.0 | +13 57 16 | 10 | 14 | 5 | 6.4 | 1.0 | 0.70 | 0.488 | | cluster + AGN($z = 0.494$) SSHARC/WARPS2 |
| RX J0907.2+3330 | 67 | 09 07 17.9 | +33 30 09 | 14 | 24 | 5 | 4.4 | 0.8 | 0.48 | 0.483 | | RDCS |
| RX J0907.3+1639 | 68 | 09 07 20.4 | +16 39 09 | 9 | 55 | 5 | 148.5 | 17.6 | 0.34 | 0.073 | 7 | A744/eBCS/EMSS |
| RX J0910.6+4248 | 69 | 09 10 39.7 | +42 48 41 | 24 | 76 | 23 | 8.3 | 2.0 | 1.24 | 0.576 | 8 | RDCS |
| RX J0921.2+4528 | 70 | 09 21 13.4 | +45 28 50 | 11 | 26 | 5 | 23.9 | 4.7 | 1.05 | 0.315 | | lenses $z = 1.66$ QSO, see § 2.3 |
| RX J0926.6+1242 | 71 | 09 26 36.6 | +12 42 56 | 9 | 16 | 3 | 16.7 | 2.1 | 1.75 | 0.489 | | |
| RX J0926.7+1234 | 72 | 09 26 45.6 | +12 34 07 | 41 | 60 | 22 | 11.7 | 3.5 | F | F | | F |
| RX J0943.5+1640 | 73 | 09 43 32.2 | +16 40 02 | 10 | 36 | 5 | 23.1 | 3.7 | 0.67 | 0.256 | | RIXOS/WARPS2 |
| RX J0943.7+1644 | 74 | 09 43 44.7 | +16 44 20 | 17 | 69 | 13 | 21.2 | 4.1 | 0.31 | 0.180 | | RIXOS/WARPS24 |
| RX J0947.7+0741 | 75 | 09 47 45.8 | +07 41 18 | 17 | 32 | 10 | 13.5 | 3.7 | 2.30 | 0.625 | | (BSHARC/SSHARC QSO $z \sim 0.63$) |
| RX J0951.7-0128 | 76 | 09 51 47.0 | -01 28 33 | 22 | 25 | 11 | 7.1 | 1.9 | 1.04 | 0.568 | 9 | WARPS1 |
| RX J0952.1-0148 | 77 | 09 52 08.7 | -01 48 18 | 18 | 39 | 14 | 9.3 | 2.5 | F | F | | F |
| RX J0953.5+4758 | 78 | 09 53 31.2 | +47 58 57 | 20 | 41 | 20 | 13.0 | 5.2 | F | F | | F |
| RX J0956.0+4107 | 79 | 09 56 03.4 | +41 07 14 | 13 | 13 | 6 | 15.6 | 3.3 | 2.34 | 0.587 | | |
| RX J0957.8+6534 | 80 | 09 57 53.2 | +65 34 30 | 12 | 19 | 5 | 9.4 | 1.7 | 1.19 | 0.530 | | |
| RX J0958.2+5516 | 81 | 09 58 13.5 | +55 16 01 | 15 | 67 | 14 | 48.2 | 7.1 | 0.97 | 0.214 | | A899 |
| RX J0959.4+4633 | 82 | 09 59 27.7 | +46 33 57 | 31 | 37 | 23 | 10.5 | 5.2 | F | F | | F |
| RX J1002.6-0808 | 83 | 10 02 40.4 | -08 08 46 | 12 | 29 | 7 | 8.6 | 2.1 | 1.07 | 0.524 | 10 | WARPS2 |
| RX J1010.2+5430 | 84 | 10 10 14.7 | +54 30 18 | 14 | 20 | 4 | 21.0 | 2.9 | 0.02 | 0.047 | 11 | RDCS/RIXOS/WARPS2 |
| RX J1011.0+5339 | 85 | 10 11 05.1 | +53 39 27 | 11 | 23 | 9 | 4.7 | 1.2 | 0.24 | 0.329 | | WARPS2 |
| RX J1011.4+5450 | 86 | 10 11 26.0 | +54 50 08 | 24 | 94 | 22 | 20.0 | 5.1 | 0.77 | 0.294 | | RDCS/RIXOS/WARPS2 |
| RX J1013.6+4933 | 87 | 10 13 38.4 | +49 33 07 | 22 | 107 | 21 | 45.6 | 9.8 | 0.36 | 0.133 | | |
| RX J1015.1+4931 | 88 | 10 15 08.5 | +49 31 32 | 10 | 14 | 8 | 10.8 | 2.6 | 0.71 | 0.383 | | |
| RX J1033.8+5703 | 89 | 10 33 51.9 | +57 03 10 | 16 | 24 | 9 | 14.5 | 4.3 | 0.01 | 0.046 | 12 | |
| RX J1036.1+5713 | 90 | 10 36 11.3 | +57 13 31 | 13 | 15 | 6 | 18.8 | 3.9 | 0.35 | 0.203 | | |
| RX J1048.0-1124 | 91 | 10 48 00.1 | -11 24 07 | 19 | 35 | 7 | 18.5 | 3.6 | 0.03 | 0.065 | | |
| RX J1049.0+5424 | 92 | 10 49 02.7 | +54 24 00 | 12 | 22 | 9 | 9.1 | 1.6 | 0.26 | 0.251 | | |
| RX J1053.3+5720 | 93 | 10 53 18.4 | +57 20 47 | 8 | 12 | 3 | 2.5 | 0.3 | 0.14 | 0.340 | 13 | RIXOS |
| RX J1056.2+4933 | 94 | 10 56 12.6 | +49 33 11 | 23 | 64 | 15 | 12.9 | 1.9 | 0.23 | 0.199 | | RIXOS/WARPS2 |
| RX J1058.2+0136 | 95 | 10 58 13.0 | +01 36 57 | 15 | 113 | 13 | 129.5 | 19.3 | 0.09 | 0.040 | 14 | A1139/eBCS/REFLEX1 |
| RX J1117.2+1744 | 96 | 11 17 12.0 | +17 44 24 | 26 | 65 | 33 | 12.0 | 5.6 | 0.50 | 0.305 | | |
| RX J1117.4+0743 | 97 | 11 17 26.1 | +07 43 35 | 12 | 18 | 7 | 6.1 | 1.6 | 0.64 | 0.477 | | WARPS2 |
| RX J1117.5+1744 | 98 | 11 17 30.2 | +17 44 44 | 16 | 36 | 10 | 14.4 | 2.5 | 1.90 | 0.548 | | |
| RX J1119.7+2126 | 99 | 11 19 43.5 | +21 26 44 | 9 | 12 | 3 | 5.5 | 0.9 | 0.01 | 0.061 | 11 | RDCS/RIXOS/WARPS2 |
| RX J1120.9+2326 | 100 | 11 20 57.9 | +23 26 41 | 16 | 29 | 8 | 21.3 | 5.0 | 2.89 | 0.562 | | |
| RX J1123.1+1409 | 101 | 11 23 10.2 | +14 09 44 | 27 | 49 | 24 | 18.2 | 4.9 | 0.93 | 0.340 | | |
| RX J1124.0-1700 | 102 | 11 24 03.8 | -17 00 11 | 22 | 34 | 19 | 10.8 | 3.4 | 0.81 | 0.407 | | |
| RX J1124.6+4155 | 103 | 11 24 36.9 | +41 55 59 | 31 | 110 | 30 | 40.1 | 9.6 | 0.67 | 0.195 | | |
| RX J1135.9+2131 | 104 | 11 35 54.5 | +21 31 05 | 17 | 72 | 20 | 17.8 | 4.0 | 0.14 | 0.133 | | |
| RX J1138.7+0315 | 105 | 11 38 43.9 | +03 15 38 | 10 | 18 | 6 | 15.9 | 3.7 | 0.11 | 0.127 | | |
| RX J1142.0+2144 | 106 | 11 42 04.6 | +21 44 57 | 26 | 56 | 34 | 45.9 | 17.4 | 0.35 | 0.131 | | |
| RX J1146.4+2854 | 107 | 11 46 26.9 | +28 54 15 | 18 | 79 | 11 | 39.2 | 5.8 | 0.38 | 0.149 | | WARPS2 |
| RX J1151.6+8104 | 108 | 11 51 40.3 | +81 04 38 | 14 | 27 | 7 | 3.7 | 1.1 | 0.15 | 0.290 | | |
| RX J1158.1+5521 | 109 | 11 58 11.7 | +55 21 45 | 9 | 21 | 5 | 4.7 | 1.0 | 0.04 | 0.135 | | |
| RX J1159.8+5531 | 110 | 11 59 51.2 | +55 31 56 | 7 | 24 | 2 | 74.2 | 7.6 | 0.21 | 0.081 | 15 | OLEG/EMSS/RDCS/RIXOS |
| RX J1200.8-0327 | 111 | 12 00 49.7 | -03 27 31 | 10 | 29 | 5 | 18.5 | 2.6 | 1.28 | 0.396 | | RIXOS/SSHARC/WARPS2 |
| RX J1204.0+2807 | 112 | 12 04 04.0 | +28 07 08 | 7 | 32 | 3 | 102.6 | 11.4 | 1.24 | 0.167 | 15 | z_{PSPC} , A1455/BSHARC/EMSS/NORAS/RDCS/RIXOS |
| RX J1204.3-0350 | 113 | 12 04 22.9 | -03 50 55 | 14 | 26 | 6 | 8.7 | 1.3 | 0.27 | 0.261 | | RDCS/SSHARC/WARPS2 |
| RX J1206.5-0744 | 114 | 12 06 33.5 | -07 44 28 | 15 | 64 | 7 | 129.0 | 16.3 | 0.26 | 0.068 | | REFLEX2 |
| RX J1211.2+3911 | 115 | 12 11 15.3 | +39 11 38 | 8 | 14 | 4 | 26.6 | 3.8 | 1.35 | 0.340 | 15 | BMW/BSHARC/EMSS/WARPS2 |
| RX J1213.5+0253 | 116 | 12 13 35.3 | +02 53 26 | 13 | 27 | 9 | 14.3 | 3.0 | 1.07 | 0.409 | | |
| RX J1216.3+2633 | 117 | 12 16 19.4 | +26 33 26 | 15 | 15 | 6 | 15.4 | 4.2 | 1.25 | 0.428 | | |
| RX J1218.4+3011 | 118 | 12 18 29.1 | +30 11 46 | 11 | 18 | 9 | 5.3 | 1.4 | 0.33 | 0.368 | | RDCS/RIXOS/WARPS2 |

TABLE 4—Continued

| Object Name | Number | α [J2000] (3) | δ [J2000] (4) | δr ["] (5) | r_c ["] (6) | δr_c ["] (7) | f_x [10^{-14} cgs] (8) | δf_x [10^{-14} cgs] (9) | L_x [10^{44} cgs] (10) | z (11) | Redshift References (12) | Notes (13) |
|-----------------|--------|----------------------------|----------------------------|--------------------------|---------------------|----------------------------|-----------------------------------|--|-----------------------------------|-------------|--------------------------------|---|
| RX J1221.4+4918 | 119 | 12 21 24.5 | +49 18 13 | 18 | 34 | 8 | 20.6 | 4.6 | 4.27 | 0.700 | | |
| RX J1222.5+0412 | 120 | 12 22 32.5 | +04 12 02 | 12 | 15 | 7 | 6.3 | 1.6 | F | F | | F |
| RX J1236.5+0051 | 121 | 12 36 31.4 | +00 51 43 | 14 | 28 | 8 | 4.8 | 1.2 | 0.09 | 0.205 | 12 | RDCS |
| RX J1237.4+1141 | 122 | 12 37 25.1 | +11 41 27 | 21 | 41 | 15 | 10.6 | 3.4 | ... | ... | | discussed in § 2.3 |
| RX J1237.6+2632 | 123 | 12 37 38.6 | +26 32 23 | 14 | 31 | 12 | 7.0 | 2.3 | 0.25 | 0.278 | | BMW |
| RX J1252.0-2920 | 124 | 12 52 05.4 | -29 20 46 | 13 | 46 | 11 | 21.7 | 4.2 | 0.34 | 0.188 | | RDCS |
| RX J1252.1-2914 | 125 | 12 52 11.3 | -29 14 59 | 8 | 11 | 5 | 8.7 | 1.6 | F | F | | F |
| RX J1254.6+2545 | 126 | 12 54 38.3 | +25 45 13 | 13 | 31 | 7 | 10.2 | 2.0 | 0.17 | 0.193 | | RDCS/WARPS2 |
| RX J1254.8+2550 | 127 | 12 54 53.6 | +25 50 55 | 12 | 40 | 8 | 13.2 | 2.5 | 0.32 | 0.233 | | RDCS/WARPS2 |
| RX J1256.0+2556 | 128 | 12 56 04.9 | +25 56 52 | 11 | 30 | 7 | 9.9 | 1.9 | 0.24 | 0.232 | | RDCS/WARPS2 |
| RX J1256.6+4715 | 129 | 12 56 39.4 | +47 15 19 | 10 | 25 | 5 | 5.7 | 0.8 | 0.43 | 0.404 | 11 | RDCS/RIXOS/WARPS2 |
| RX J1301.7+1059 | 130 | 13 01 43.6 | +10 59 33 | 18 | 54 | 11 | 28.1 | 5.6 | 0.66 | 0.231 | | |
| RX J1309.9+3222 | 131 | 13 09 55.6 | +32 22 31 | 23 | 42 | 19 | 9.0 | 2.9 | 0.34 | 0.290 | | |
| RX J1311.2+3228 | 132 | 13 11 12.8 | +32 28 58 | 8 | 22 | 3 | 46.7 | 5.8 | 1.22 | 0.245 | 15 | BSHARC/EMSS/RIXOS/WARPS2 |
| RX J1311.5-0551 | 133 | 13 11 30.2 | -05 51 26 | 20 | 36 | 6 | 13.7 | 2.4 | 1.29 | 0.461 | | |
| RX J1325.2+6550 | 134 | 13 25 14.9 | +65 50 29 | 28 | 54 | 21 | 10.1 | 3.1 | 0.15 | 0.180 | | z_{PSPC} , WARPS2 |
| RX J1325.7-2943 | 135 | 13 25 43.9 | -29 43 51 | 17 | 43 | 11 | 7.7 | 2.7 | F | F | | F |
| RX J1329.4+1143 | 136 | 13 29 27.3 | +11 43 31 | 22 | 120 | 16 | 97.0 | 16.6 | 0.02 | 0.024 | 16 | NGC 5171 group |
| RX J1334.5-0822 | 137 | 13 34 31.1 | -08 22 29 | 10 | 13 | 5 | 5.2 | 1.1 | F | F | | F |
| RX J1334.5+3756 | 138 | 13 34 34.4 | +37 56 58 | 11 | 16 | 5 | 1.6 | 0.3 | 0.07 | 0.308 | 17 | |
| RX J1335.0+3750 | 139 | 13 35 03.7 | +37 50 00 | 9 | 21 | 4 | 2.9 | 0.4 | 0.20 | 0.382 | 17 | RDCS |
| RX J1336.7+3837 | 140 | 13 36 42.1 | +38 37 32 | 16 | 20 | 9 | 5.9 | 1.6 | 0.09 | 0.180 | | |
| RX J1337.8+4815 | 141 | 13 37 48.3 | +48 15 46 | 10 | 16 | 4 | 7.1 | 1.5 | F | F | | F |
| RX J1337.8+2638 | 142 | 13 37 50.4 | +26 38 49 | 12 | 21 | 6 | 9.6 | 2.1 | 0.51 | 0.342 | | WARPS2 |
| RX J1337.8+3854 | 143 | 13 37 53.3 | +38 54 09 | 17 | 32 | 9 | 14.3 | 3.6 | 0.41 | 0.252 | | |
| RX J1340.5+4017 | 144 | 13 40 33.5 | +40 17 47 | 10 | 19 | 5 | 16.1 | 2.5 | 0.21 | 0.171 | 18 | OLEG |
| RX J1340.8+3958 | 145 | 13 40 53.7 | +39 58 11 | 19 | 66 | 16 | 34.4 | 6.9 | 0.44 | 0.169 | 19 | A1774 |
| RX J1341.8+2622 | 146 | 13 41 51.7 | +26 22 54 | 8 | 103 | 4 | 814.0 | 84.6 | 1.80 | 0.072 | 20 | A1775/BCS/NORAS/RBS |
| RX J1342.0+5200 | 147 | 13 42 05.0 | +52 00 37 | 13 | 10 | 4 | 12.4 | 1.9 | F | F | | F |
| RX J1342.8+4028 | 148 | 13 42 49.1 | +40 28 11 | 16 | 15 | 6 | 7.4 | 2.0 | 1.62 | 0.699 | | WARPS2 |
| RX J1343.4+4053 | 149 | 13 43 25.0 | +40 53 14 | 10 | 18 | 7 | 12.6 | 2.8 | 0.11 | 0.140 | | |
| RX J1343.4+5547 | 150 | 13 43 29.0 | +55 47 17 | 23 | 109 | 17 | 17.5 | 2.8 | 0.04 | 0.069 | | RIXOS |
| RX J1354.2-0221 | 151 | 13 54 16.9 | -02 21 47 | 11 | 27 | 4 | 14.5 | 2.6 | 1.89 | 0.546 | | RDCS/SSHARC |
| RX J1354.8+6917 | 152 | 13 54 49.1 | +69 17 20 | 15 | 26 | 10 | 6.4 | 1.9 | 0.13 | 0.207 | | |
| RX J1406.2+2830 | 153 | 14 06 16.3 | +28 30 52 | 9 | 14 | 4 | 8.5 | 1.2 | 1.14 | 0.546 | 21 | RDCS/WARPS1 |
| RX J1406.9+2834 | 154 | 14 06 54.9 | +28 34 17 | 8 | 30 | 3 | 25.7 | 3.2 | 0.16 | 0.118 | 21 | BMW/BSHARC/RDCS/WARPS1 |
| RX J1410.2+5942 | 155 | 14 10 12.4 | +59 42 40 | 18 | 38 | 12 | 33.5 | 5.1 | 0.92 | 0.250 | 22 | probably part of A1877 |
| RX J1410.2+5938 | 156 | 14 10 15.2 | +59 38 31 | 17 | 31 | 22 | 20.1 | 8.7 | 0.56 | 0.250 | 22 | probably part of A1877 |
| RX J1415.6+1906 | 157 | 14 15 37.9 | +19 06 33 | 13 | 52 | 5 | 25.4 | 3.4 | ... | ... | | obscured by Arcturus |
| RX J1416.4+4446 | 158 | 14 16 28.7 | +44 46 41 | 8 | 16 | 4 | 40.4 | 5.2 | 2.77 | 0.400 | | |
| RX J1418.5+2510 | 159 | 14 18 31.1 | +25 10 50 | 7 | 33 | 1 | 75.6 | 7.8 | 2.84 | 0.296 | 9 | BMW/BSHARC/RDCS/WARPS1 |
| RX J1418.7+0644 | 160 | 14 18 45.2 | +06 44 02 | 9 | 18 | 5 | 16.4 | 3.0 | F | F | | F |
| RX J1419.3+0638 | 161 | 14 19 23.5 | +06 38 42 | 9 | 17 | 4 | 13.1 | 1.9 | 1.90 | 0.574 | 10 | WARPS2 |
| RX J1419.9+0634 | 162 | 14 19 57.2 | +06 34 26 | 15 | 35 | 7 | 10.3 | 2.1 | 1.38 | 0.549 | 10 | WARPS2 |
| RX J1429.6+4234 | 163 | 14 29 38.1 | +42 34 25 | 26 | 35 | 12 | 8.5 | 2.4 | F | F | | F |
| RX J1438.9+6423 | 164 | 14 38 55.5 | +64 23 44 | 19 | 103 | 11 | 26.2 | 3.6 | 0.25 | 0.146 | | BMW |
| RX J1444.1+6344 | 165 | 14 44 07.7 | +63 44 58 | 15 | 26 | 9 | 17.4 | 3.2 | 0.69 | 0.299 | 22 | z_{PSPC} , A1969 |
| RX J1500.0+2233 | 166 | 15 00 02.7 | +22 33 51 | 24 | 37 | 17 | 14.5 | 4.5 | 0.35 | 0.230 | | z_{PSPC} |
| RX J1500.8+2244 | 167 | 15 00 51.5 | +22 44 41 | 16 | 31 | 10 | 17.8 | 4.2 | 1.58 | 0.450 | | |
| RX J1515.5+4346 | 168 | 15 15 32.5 | +43 46 39 | 18 | 60 | 19 | 34.6 | 9.7 | 0.29 | 0.137 | | |
| RX J1515.6+4350 | 169 | 15 15 36.8 | +43 50 50 | 22 | 34 | 18 | 10.5 | 3.8 | 0.28 | 0.243 | | |
| RX J1524.6+0957 | 170 | 15 24 40.3 | +09 57 39 | 9 | 26 | 3 | 30.4 | 4.1 | 3.45 | 0.516 | | cl + group ($z = 0.078$), BSHARC/WARPS2 |
| RX J1537.7+1200 | 171 | 15 37 44.3 | +12 00 26 | 30 | 84 | 26 | 26.4 | 7.4 | 0.21 | 0.134 | | |
| RX J1540.8+1445 | 172 | 15 40 53.3 | +14 45 34 | 13 | 17 | 8 | 7.6 | 2.0 | 0.68 | 0.441 | | |
| RX J1544.0+5346 | 173 | 15 44 05.0 | +53 46 27 | 19 | 35 | 11 | 9.7 | 2.2 | 0.05 | 0.112 | | |
| RX J1547.3+2056 | 174 | 15 47 20.7 | +20 56 50 | 24 | 51 | 20 | 25.4 | 7.0 | 0.79 | 0.266 | | z_{PSPC} |
| RX J1552.2+2013 | 175 | 15 52 12.3 | +20 13 45 | 9 | 59 | 7 | 49.5 | 6.0 | 0.40 | 0.136 | | BSHARC/WARPS1 |
| RX J1606.7+2329 | 176 | 16 06 42.5 | +23 29 00 | 12 | 34 | 13 | 12.1 | 2.8 | 0.53 | 0.310 | | WARPS2 |
| RX J1620.3+1723 | 177 | 16 20 22.0 | +17 23 05 | 12 | 35 | 8 | 20.8 | 3.7 | 0.12 | 0.112 | | z_{PSPC} |

TABLE 4—Continued

| Object Name | Number | α [J2000] (3) | δ [J2000] (4) | δr [′′] (5) | r_c [′′] (6) | δr_c [′′] (7) | f_x [10^{-14} cgs] (8) | δf_x [10^{-14} cgs] (9) | L_x [10^{44} cgs] (10) | z (11) | Redshift References (12) | Notes (13) |
|-----------------|--------|----------------------------|----------------------------|---------------------------|----------------------|-----------------------------|-----------------------------------|--|-----------------------------------|-------------|--------------------------------|----------------------------------|
| RX J1629.7+2123 | 178 | 16 29 46.1 | +21 23 54 | 19 | 46 | 8 | 25.3 | 4.0 | 0.38 | 0.184 | | |
| RX J1630.2+2434 | 179 | 16 30 15.2 | +24 34 59 | 23 | 129 | 13 | 179.4 | 25.9 | 0.33 | 0.066 | | MCG +04-39-010 group |
| RX J1631.0+2122 | 180 | 16 31 04.6 | +21 22 02 | 16 | 58 | 14 | 29.1 | 6.4 | 0.12 | 0.098 | | |
| RX J1633.6+5714 | 181 | 16 33 40.0 | +57 14 37 | 14 | 24 | 8 | 3.5 | 0.7 | 0.09 | 0.239 | | RDCS/RIXOS/WARPS2 |
| RX J1639.9+5347 | 182 | 16 39 55.6 | +53 47 56 | 12 | 170 | 8 | 130.5 | 14.8 | 0.69 | 0.111 | 23 | A2220/WARPS2 |
| RX J1641.1+8232 | 183 | 16 41 10.0 | +82 32 27 | 13 | 78 | 11 | 80.5 | 10.9 | 1.48 | 0.206 | | TTR95 1646+82 cluster, BSHARC |
| RX J1641.8+4001 | 184 | 16 41 52.5 | +40 01 29 | 24 | 51 | 15 | 29.4 | 7.8 | 2.72 | 0.464 | | |
| RX J1642.5+3959 | 185 | 16 42 33.5 | +39 59 05 | 12 | 19 | 9 | 5.3 | 1.4 | F | F | | F, QSO 1640+400 $z = 1.59$ |
| RX J1642.6+3935 | 186 | 16 42 38.9 | +39 35 53 | 16 | 27 | 9 | 10.1 | 2.3 | 0.58 | 0.355 | | |
| RX J1658.5+3430 | 187 | 16 58 34.7 | +34 30 12 | 16 | 58 | 10 | 33.6 | 5.2 | 1.60 | 0.330 | | |
| RX J1659.7+3410 | 188 | 16 59 44.6 | +34 10 17 | 16 | 25 | 11 | 9.8 | 3.4 | 0.52 | 0.341 | | |
| RX J1700.7+6413 | 189 | 17 00 42.3 | +64 13 00 | 7 | 18 | 1 | 45.6 | 4.7 | 1.01 | 0.225 | 24 | A2246/NORAS/RDCS |
| RX J1701.3+6414 | 190 | 17 01 23.0 | +64 14 11 | 7 | 25 | 2 | 38.6 | 4.2 | 3.38 | 0.453 | | RDCS/BSHARC |
| RX J1701.7+6421 | 191 | 17 01 46.1 | +64 21 15 | 14 | 32 | 8 | 3.5 | 0.7 | 0.08 | 0.220 | | RDCS |
| RX J1702.2+6420 | 192 | 17 02 13.3 | +64 20 00 | 12 | 32 | 7 | 6.3 | 1.2 | 0.15 | 0.224 | | RDCS/WARPS2 |
| RX J1722.8+4105 | 193 | 17 22 53.8 | +41 05 25 | 22 | 42 | 12 | 29.4 | 6.5 | 1.23 | 0.309 | | |
| RX J1729.0+7440 | 194 | 17 29 01.9 | +74 40 46 | 40 | 100 | 31 | 17.3 | 7.2 | 0.35 | 0.213 | | |
| RX J1746.4+6848 | 195 | 17 46 29.1 | +68 48 54 | 13 | 56 | 10 | 22.3 | 3.2 | 0.47 | 0.217 | | RDCS/WARPS2 |
| RX J2003.4-5556 | 196 | 20 03 28.4 | -55 56 47 | 8 | 16 | 2 | 47.6 | 6.3 | 0.00 | 0.015 | 5 | Abell S840 |
| RX J2004.8-5603 | 197 | 20 04 49.4 | -56 03 44 | 16 | 30 | 11 | 10.4 | 2.5 | F | F | | F |
| RX J2005.2-5612 | 198 | 20 05 13.6 | -56 12 58 | 9 | 7 | 3 | 35.0 | 4.9 | F | F | | F |
| RX J2059.9-4245 | 199 | 20 59 55.2 | -42 45 33 | 8 | 9 | 3 | 11.2 | 1.8 | 0.53 | 0.323 | | |
| RX J2108.8-0516 | 200 | 21 08 51.2 | -05 16 49 | 12 | 34 | 7 | 11.6 | 1.7 | 0.53 | 0.319 | | BMW/RDCS/SSHARC/WARPS1 |
| RX J2114.3-6800 | 201 | 21 14 20.4 | -68 00 56 | 13 | 17 | 3 | 25.8 | 3.3 | 0.19 | 0.130 | 25 | OLEG/RDCS/SSHARC |
| RX J2137.1+0026 | 202 | 21 37 06.7 | +00 26 51 | 21 | 55 | 20 | 27.8 | 5.7 | 0.03 | 0.051 | 26 | UGC 11780 group |
| RX J2139.9-4305 | 203 | 21 39 58.5 | -43 05 14 | 15 | 12 | 6 | 8.3 | 2.0 | 0.54 | 0.376 | | |
| RX J2146.0+0423 | 204 | 21 46 04.8 | +04 23 19 | 13 | 17 | 2 | 13.8 | 2.1 | 1.71 | 0.531 | | |
| RX J2202.7-1902 | 205 | 22 02 44.9 | -19 02 10 | 22 | 36 | 9 | 6.6 | 2.2 | 0.58 | 0.438 | | RDCS/SSHARC/WARPS2 |
| RX J2212.6-1713 | 206 | 22 12 38.2 | -17 13 55 | 12 | 22 | 13 | 5.4 | 1.4 | 0.04 | 0.134 | | z_{PSPC} |
| RX J2213.5-1656 | 207 | 22 13 31.0 | -16 56 11 | 17 | 41 | 12 | 18.1 | 3.2 | 0.71 | 0.297 | | |
| RX J2239.4-0547 | 208 | 22 39 24.7 | -05 47 04 | 13 | 11 | 2 | 22.2 | 3.5 | 0.58 | 0.242 | 9 | A2465S/WARPS1 |
| RX J2239.5-0600 | 209 | 22 39 34.4 | -06 00 14 | 19 | 21 | 10 | 5.9 | 2.0 | 0.08 | 0.173 | | WARPS1 |
| RX J2239.6-0543 | 210 | 22 39 38.9 | -05 43 18 | 15 | 34 | 5 | 32.4 | 5.0 | 0.84 | 0.243 | 9 | A2465N/WARPS1 |
| RX J2247.4+0337 | 211 | 22 47 29.1 | +03 37 13 | 20 | 46 | 17 | 23.0 | 6.3 | 0.41 | 0.200 | | OLEG |
| RX J2257.8+2056 | 212 | 22 57 49.4 | +20 56 25 | 11 | 22 | 7 | 11.1 | 2.1 | 0.44 | 0.297 | | WARPS2 |
| RX J2258.1+2055 | 213 | 22 58 07.1 | +20 55 07 | 9 | 24 | 3 | 50.5 | 6.1 | 1.81 | 0.288 | 15 | Zw2255.5+2041/BSHARC/EMSS/WARPS2 |
| RX J2305.4-3546 | 214 | 23 05 26.2 | -35 46 01 | 15 | 55 | 14 | 15.5 | 3.4 | 0.28 | 0.201 | | |
| RX J2305.4-5130 | 215 | 23 05 26.6 | -51 30 30 | 17 | 21 | 10 | 4.2 | 1.4 | 0.07 | 0.194 | | RDCS |
| RX J2318.0-4235 | 216 | 23 18 04.8 | -42 35 30 | 17 | 28 | 8 | 15.5 | 2.7 | 0.30 | 0.209 | | BMW |
| RX J2319.5+1226 | 217 | 23 19 33.9 | +12 26 17 | 10 | 30 | 6 | 38.2 | 4.7 | 0.27 | 0.126 | | RIXOS/WARPS1 |
| RX J2325.6-5443 | 218 | 23 25 39.1 | -54 43 59 | 35 | 91 | 26 | 22.4 | 7.7 | 0.10 | 0.102 | | |
| RX J2328.8+1453 | 219 | 23 28 49.9 | +14 53 12 | 21 | 27 | 12 | 7.6 | 1.7 | 0.85 | 0.497 | | WARPS2 |
| RX J2331.8-3747 | 220 | 23 31 52.1 | -37 47 11 | 28 | 46 | 25 | 10.8 | 4.7 | 0.38 | 0.280 | | |
| RX J2348.8-3117 | 221 | 23 48 53.7 | -31 17 20 | 12 | 43 | 8 | 32.5 | 5.1 | 0.49 | 0.184 | | A4043 |
| RX J2349.1-3122 | 222 | 23 49 07.6 | -31 22 26 | 11 | 21 | 6 | 6.0 | 1.4 | F | F | | F |
| RX J2355.1-1500 | 223 | 23 55 11.8 | -15 00 26 | 26 | 70 | 20 | 26.6 | 6.7 | 0.09 | 0.086 | | |

Note. — Units of right ascension are hours, minutes, and seconds, and units of declination are degrees, arcminutes, and arcseconds. Units of X-ray flux are 10^{-14} erg cm^{-2} s^{-1} and units of X-ray luminosity are 10^{44} h_{50}^2 erg s^{-1} , both of which are in the 0.5–2.0 keV energy band. Redshift references — (1) Couch et al. 1991; (2) Quintana & Ramirez 1995; (3) Loveday et al. 1996; (4) Nesci & Altamore 1990; (5) Abell, Corwin, & Olowin 1989; (6) Rosati et al. 1999; (7) Kurtz et al. 1985; (8) P. Rosati (private communication); (9) Perlman et al. 2002; (10) H. Ebeling (private communication); (11) Mason et al. 2000; (12) J. Huchra (private communication); (13) Schmidt et al. 1998; (14) Struble & Rood 1999; (15) Stocke et al. 1991; (16) Mahdavi et al. 2000; (17) McHardy et al. 1998; (18) Ponman et al. 1994; (19) Kopylov, Fetisova, & Shvartsman 1984; (20) Oegerle, Hill, & Fitchett 1995; (21) Boyle, Wilkes, & Elvis 1997; (22) Huchra et al. 1990; (23) Ulrich 1976; (24) Schneider, Gunn, & Hoessel 1983; (25) Griffiths et al. 1992; (26) Huchra, Vogeley, & Geller 1999. Table 4 is also available in machine-readable form in the electronic edition of the *Astrophysical Journal*.

TABLE 5
160SD CLUSTER MEMBERSHIPS IN OTHER SURVEYS

| Other Survey | Coincidences with 160SD | Percentage of 160SD | Percentage of Other Survey | Sample Size of Other Survey | Parent Dataset of Other Survey |
|--------------|-------------------------|---------------------|----------------------------|-----------------------------|--------------------------------|
| BCS | 1 | 0.5 % | 0.5 % | 201 | RASS |
| eBCS | 2 | 1.0 % | 2.0 % | 99 | RASS |
| BMW-HRI | 9 | 4.5 % | 6.0 % | ~150 | <i>ROSAT</i> HRI |
| BSHARC | 12 | 6.0 % | 32.4 % | 37 | <i>ROSAT</i> PSPC |
| CIZA | 0 | ... | ... | 150 | RASS |
| EMSS | 6 | 3.0 % | 6.7 % | 89 | <i>Einstein</i> IPC |
| MACS | 0 | ... | ... | 120 | RASS |
| NEP | 0 | ... | ... | 63 | RASS |
| NORAS | 3 | 1.5 % | 0.8 % | 378 | RASS |
| RASS1BS | 0 | ... | ... | 126 | RASS |
| RBS | 1 | 0.5 % | 0.5 % | 186 | RASS |
| RDCS | 46 | 22.9 % | 36.5 % | 126 | <i>ROSAT</i> PSPC |
| REFLEX-I | 1 | 0.5 % | 0.2 % | 452 | RASS |
| REFLEX-II | 3 | 1.5 % | 0.8 % | ~375 | RASS |
| RIXOS | 18 | 9.0 % | 58.0 % | 31 | <i>ROSAT</i> PSPC |
| SGP | 0 | ... | ... | 186 | RASS |
| SSHARC | 9 | 4.4 % | 28.1 % | 32 | <i>ROSAT</i> PSPC |
| WARPS-I | 16 | 8.0 % | 47.1 % | 34 | <i>ROSAT</i> PSPC |
| WARPS-II | 44 | 21.9 % | 35.5 % | 124 | <i>ROSAT</i> PSPC |